Title: T cell responses induced by SARS-CoV-2 mRNA vaccination are associated with clonal replacement

Authors: Hiroyasu Aoki[1,2], Masahiro Kitabatake[3], Haruka Abe[1], Shigeyuki Shichino[1], Atsushi Hara[3], Noriko Ouji-Sageshima[3], Toshihiro Ito[3], Kouji Matsushima[1], and Satoshi Ueha[1]*

Affiliations:

[1]Division of Molecular Regulation of Inflammatory and Immune Diseases, Research Institute for Biomedical Sciences, Tokyo University of Science, Chiba, Japan.

[2]Department of Preventive Medicine, Graduate School of Medicine, The University of Tokyo.

[3]Department of Immunology, Nara Medical University, Nara, Japan.

* Satoshi Ueha, Ph.D., Division of Molecular Regulation of Inflammatory and Immune Diseases, Research Institute for Biomedical Sciences, Tokyo University of Science, 2669 Yamazaki, Noda City Chiba, 278-0022, Japan

E-mail; ueha@rs.tus.ac.jp

Abstract: mRNA vaccines against the Spike glycoprotein of severe acute respiratory syndrome type 2 coronavirus (SARS-CoV-2) elicit strong T-cell responses. However, it is unknown whether T cell clones induced by the first vaccination or newly generated T cell clones dominate responses to the secondary vaccination. Here, we analyzed the kinetic profile of Spike-reactive T-cell clones before the first dose, one week after the first and second dose, and four weeks after the second dose of the BNT162b mRNA vaccine. Interestingly, a new set of Spike-reactive $CD8^+$ T cell clones exhibited the greatest expansion following secondary vaccination and replaced the clones that had responded to the primary vaccination. Single-cell mRNA/protein/TCR analysis revealed that the first-responder clones exhibited a terminally differentiated phenotype, whereas second-responder clones exhibited an actively proliferating phenotype. These results show that Spike-reactive T cell responses induced by repetitive mRNA vaccination are augmented and maintained by replacement with newly−generated clones with proliferative potential.

One Sentence Summary: TCR repertoire analysis following mRNA vaccination against SARS-CoV-2 revealed the replacement of Spike-reactive T cell clones.

Main Text:

INTRODUCTION

mRNA vaccines against Spike glycoprotein of severe acute respiratory syndrome type 2 coronavirus (SARS-CoV-2), including Pfizer-BioNTech's BNT162b and Moderna's mRNA-1273, are strikingly effective at reducing coronavirus disease 2019 (COVID-19) (*1*). These mRNA vaccines elicit both humoral and cellular immune responses specific for the viral Spike protein (*2–4*). Studies on the cellular immune responses following SARS-CoV-2 mRNA vaccination have demonstrated that the numbers of Spike-reactive T cells increase in the peripheral blood after the first dose, and are additionally boosted after the second dose (*4–6*). The cellular immune response may be more protective to variants of concerns (VOCs) of SARS-CoV-2 than the humoral response, because it can target relatively conserved regions of the Spike protein (*7*, *8*).

Previous studies demonstrated that secondary, or boost, vaccinations induce the reactivation of memory $CD8^+$ T cells established following the initial vaccination (*9–12*). However, repetitive antigen stimulation in mice alters the properties of memory T cells, including enhancement of their effector function, and reductions in the proliferation potential and ability to produce IL-2 (*10*, *13*). This suggests that memory $CD8^+$ T cells induced by the first vaccination become poorly, or non-responsive in the course of repetitive antigen stimulation. In line with this hypothesis, we previously reported that older memory T cell populations were replaced by newly generated T cell populations in a serial adoptive transfer model characterized by repetitive antigen exposure (*14*). However, in repetitive SARS-CoV-2 mRNA vaccinations, it is not known whether T cell clones induced by the first vaccination or newly generated clones dominate responses to subsequent vaccination.

Pathogen-reactive T cells recognize distinct antigenic epitopes via their unique T cell receptor (TCR). To analyze changes in T cell clonal dominance during SARS-CoV-2 mRNA vaccination, we undertook a longitudinal repertoire analysis by TCR sequencing. This enabled us to comprehensively quantify the changes in the frequencies of specific T-cell clones ("kinetic profile") during primary and secondary responses to mRNA vaccination. Specifically, we performed a longitudinal TCR repertoire analysis on peripheral blood T cells at four time points before and after the BNT162b mRNA vaccination. Spike-reactive T-cell clones were identified by an activation-induced marker assay (AIM assay) using a Spike peptide pool, and their response kinetics were analyzed by tracking their TCRs in longitudinal repertoire data. Furthermore, we matched the kinetics of the clonal response with immunological phenotype using single-cell analysis of gene expression and TCR sequence. These analyses revealed that Spike-reactive T-cell responses induced by secondary mRNA vaccination resulted in the replacement of Spike-reactive T-cell clones from the primary response with new clones that exhibited different response characteristics.

RESULTS

Transient expansion of $CD8^+$ T cell clones was prominent after the second vaccination

To analyze the kinetics of T cell clones following mRNA vaccination to SARS-CoV-2, we studied a cohort of 41 healthcare workers at Nara Medical University (Japan) who had received two doses of the Pfizer-BNT162b2 vaccine (*15*). Peripheral blood mononuclear cell (PBMC) samples were collected from the participants at four points: before the first dose (point 1: P1), seven days after the first dose (P2), seven days after the second dose (P3), and 28 days after the second dose (P4) (Fig. 1A). $CD4^+$ and $CD8^+$ T cells were separated from the PBMC sample, then their TCR repertoire was analyzed ("bulk TCR repertoire analysis").

To identify the kinetic profiles of T-cell clones, we applied weighted gene correlation network analysis (WGCNA) on the longitudinal bulk TCR repertoire dataset (*16*) (Fig. 1D, method). From the kinetic profile of the top 150 clones detected at four points (which occupied about 45% of $CD8^+$ and 10% of $CD4^+$ repertoire on average, fig. S1A), we identified twelve, and ten patterns, of kinetic profile in the $CD8^+$ and $CD4^+$ repertoires (Fig. 1C and fig. S1B-D). $CD8^+$ module Green (+) and $CD4^+$ module Turquoise (+) were the modules that increased at P2 and then decreased, corresponding to a transient expansion after the first dose (hereafter "first-responders"). $CD8^+$ and $CD4^+$ module Brown (+) were the modules that transiently increased at P3 and then decreased (hereafter "second-responders"). $CD8^+$ module Turquoise (+) and $CD4^+$ module Green (+) were modules that increased at P4: four weeks after the second dose (hereafter "long-term responders").

These modules were robustly identified regardless of the number of top $CD8^+/CD4^+$ clones used for WGCNA analysis (fig. S1E and F).

We next classified individual clones within the kinetic profile patterns and calculated their total frequency at each of the four points (fig. S2A-D). Second and long-term responders seemed to be dominant in patterns at P3, and P4, respectively. Moreover, the extent of clonal response of each pattern during vaccination, defined by the maximum changes in the total frequency through P1 to P4, was more significant in second-responders than first- and long-term responders (first-responders: 2.52%, second-responders: 12.93%, long-term responders: 5.72%, median) (Fig. 1E). These results suggest that the $CD8^+$ T cells responded more strongly after the second vaccination than the first vaccination.

We also analyzed the $CD4^+$ T cell repertoire. First- and second-responders tended to predominate at P2, and P3, respectively (Fig. 2A and fig. S2E-H). The clonal expansion of first-responders was greater than that of other patterns, followed by second-responders (first-responders: 11.86%, second-responders: 8.63%, long-term responders: 2.94%, median) (Fig. 2B). These data suggest that the clonal response of $CD4^+$ T cells to vaccination was characterized by the greater clonal expansion after the first dose.

Spike-reactive $CD8^+$ T cell clones were induced after vaccination

Next, we analyzed whether vaccination induced Spike-reactive $CD8^+$ T cells. We utilized the public database of SARS-CoV-2-reactive TCRs (*17–19*) and searched for biochemically similar TCRs to our dataset (*20*). In brief, we formed TCR meta-clonotypes for each SARS-CoV-2 epitope (groups of TCRs sharing similar complementarity determining regions, based on TCRs reported in the three articles). We then searched for TCRs conforming to these meta-clonotypes in our dataset. On average, 35 clones per participant belonged to SARS-Cov2-reactive meta-clonotypes. Furthermore, the frequency of clones belonging to each SARS-CoV-2 protein meta-clonotype was determined (Fig. 3A). The total frequency of Spike-reactive meta-clonotypes was significantly increased at P2 and P3 (Fig. 3B). On the other hand, the total frequency of meta-clonotypes reactive to other SARS-CoV-2 proteins remained almost constant following vaccination (Fig. 3B). This result demonstrated that mRNA vaccination induced a $CD8^+$ T cell response to Spike, but not to other SARS-CoV-2 proteins.

We next investigated whether individual $CD8^+$ T cell clones with Spike-reactive meta-clonotypes were expanded after vaccination. Of 1,421 clones in Spike-reactive meta-clonotypes in 41 participants, only 140 clones were detected at more than two points. The distribution of WGCNA modules (Fig. 1C) among these 140 clones was assessed and compared to that among clones in other meta-clonotypes. This comparison revealed that first- and second-responders were enriched among clones with Spike-reactive meta-clonotypes, while long-term responders were not (Fig. 3C). Moreover, the module Yellow (-), which peaked at P3 like second-responders, was also enriched in Spike-reactive meta-clonotypes. These three modules occupied about 60% of clones with Spike-reactive meta-clonotypes. This result suggested that Spike-reactive T cell clones reported in the public database were also expanded in our cohort after the first or second vaccination.

Spike-reactive $CD8^+$ T-cell clones were replaced following secondary vaccination

To detect Spike-reactive clones that were not covered in the public database, we analyzed the repertoire of Spike-reactive T cells in our participants. For this purpose, an activation-induced marker (AIM) assay was performed on 15 participants (*5*, *21–23*). PBMCs collected at P3 were

stimulated with peptide pools of the SARS-CoV-2 Spike protein. Then, CD137$^+$ or CD107a$^+$ non-naïve CD8$^+$ T cells, and CD40L$^+$ CD69$^+$ non-naive CD4$^+$ T cells were sorted as AIM$^+$ Spike-reactive cells (Fig. 4A). We sequenced the TCRs of AIM$^+$ and AIM$^-$ non-naive T cells and identified AIM$^+$ CD8$^+$ and CD4$^+$ T cell clones (fig. S3A). Then, we excluded Spike-nonreactive clones that became AIM+ during co-culture ("by-stander" clones) based on their enrichment in the AIM$^+$ repertoire relative to the AIM$^-$ repertoire (Fig. 4B and C, and fig. S3B and C). Notably, the total frequency of AIM$^+$ clones is significantly higher than the proportion of AIM$^+$ cells among CD4$^+$ or CD8$^+$ T cells (fig. S3D). This indicated that Spike-reactive clones included T cells that did not become AIM$^+$, which is consistent with the fact that the AIM assay underestimates the frequency of Spike-reactive T cells (*2*). Next, these AIM$^+$ clones were tracked in the whole TCR repertoire dataset from P1 to P4. We observed that the total frequency of AIM$^+$ clones increased at P3 and then decreased at P4 (Fig. 4D and fig. S3E), which is consistent with the kinetics of Spike-reactive T cells through vaccination reported in the previous studies (*4–6*).

To analyze the kinetic profile of AIM$^+$ clones, we assigned AIM$^+$ and AIM$^-$ clones into WGCNA modules as in Fig.1 and compared the proportion of each module (Fig. 4E, left). This classification revealed that the proportion of second-responders was significantly higher in AIM$^+$ clones than in AIM$^-$ ones, while first- and long-term responders were not (Fig. 4E, right). In the CD8$^+$ T cell repertoire, the expansion of second-responders was remarkable. Thus, we investigated whether AIM$^+$ clones were enriched in second-responders. The proportion of AIM$^+$ clones among second-responders at P3 varied between participants (0.4% - 70.8%); however, the participants where the frequency of AIM$^+$ clones at P3 was higher than the median ("AIM-high participants") exhibited a significantly higher proportion of AIM$^+$ clones among second-responders (fig. S3D and Fig. 4F). On the other hand, in the AIM-low participants, the frequency of AIM$^+$ second-responder clones was low, irrespective of the total frequency of second-responders (Fig.4G). These results suggested that the expansion of AIM$^+$ clones as second-responders was necessary to induce greater anti-Spike CD8$^+$ T cell response following the vaccination.

Next, we investigated whether second-responders also predominated among the AIM$^+$ clones at other time points (Fig. 4H and fig. S4A-D). As expected, the total frequency of AIM$^+$ second-responders was the highest in nine out of the fourteen (9/14) participants at P3 (fig. S3B). However, at P2, the AIM$^+$ second-responders tended to be less dominant than AIM$^+$ first- and long-term responders (fig. S3B). In addition, at P4, AIM$^+$ second-responders was nearly equivalent to AIM$^+$ long-term responders (+) (fig. S3D). These results suggest that AIM$^+$ second-responders were not dominant before, or four weeks after, the second vaccine dose. Moreover, at the clonal level, only 51% and 67% of the top 10 most expanded AIM$^+$ clones at P3 remained top 10 at P2 and P4, respectively. Namely, half of the top 10 AIM$^+$ clones were replaced between P2 and P3, and one-third were replaced between P3 and P4 (Fig. 4I). In summary, these results suggest that the increase in Spike-reactive CD8$^+$ T cells by vaccination was accompanied by the replacement of T cell clones between the first and the second dose.

We also analyzed the kinetics of AIM$^+$ clones in the CD4$^+$ T cell repertoire. The proportion of first- and second-responders was significantly higher in AIM$^+$ clones (Fig. 5A). Moreover, AIM-high participants showed a higher proportion of AIM$^+$ clones among first- and second-responders at P2 or P3, as observed in the CD8$^+$ repertoire (Fig. 5B). However, the proportion of AIM$^+$ clones was much smaller in the CD4$^+$ repertoire than in CD8$^+$ (-10% for first-responder and -40% for second-responder). The dominant patterns of AIM$^+$ clones were replaced between time points in the CD4$^+$ repertoire, as observed in CD8$^+$ (Fig. 5C and fig.S4E-H). Furthermore, at the clonal level,

172 only 35 % and 45 % of the top 10 most expanded AIM$^+$ clones at P3 remained top 10 at P2 and
173 P4, respectively (Fig. 5D). These results indicate that CD4$^+$ Spike-reactive clones were also
174 replaced after the first and the second vaccination.

175 **First- and second-responder clones differ in their phenotype after the second vaccination.**

176 From TCR repertoire analysis, we have determined that the T-cell clones that expanded after the
177 first vaccination ("first-responder") were different from those expanded after the second
178 vaccination ("second-responder"). This observation suggests that the first-responder clones could
179 not expand as much as second-responder clones after the second vaccination. However, it remained
180 unclear whether the phenotype of first-responders after the second vaccination differed from that
181 of second-responders. To address this question, the gene-expression profiles of first- and second-
182 responder clones after the second dose was analyzed. We performed targeted single-cell RNA-seq
183 (scRNA-seq) combined with single-cell TCR sequencing (scTCR-seq) and protein expression
184 analysis using oligo-conjugated antibodies (AbSeq) on non-naive CD4$^+$ and CD8$^+$ T cells collected
185 at P3 from the two participants (ID2 and ID27) (fig. S5A). Unsupervised clustering using
186 integrated data of mRNA and surface protein (*24*) identified six clusters in non-naive CD8$^+$ T cells
187 (Fig6A-C, and fig. S5B-D). Clusters 2 and 3 (terminally differentiated: TD) were characterized by
188 high expression of *GZMB* and CD45RA (*25*, *26*), and cluster 0 (innate-like: IL) expressed *ZBTB16*
189 and CD161 (*27*). Semi-invariant TCRα chains are typically present in mucosal-associated invariant
190 T cells (MAIT) (*28–30*), TRAV1-2/TRAJ33, TRAV1-2/TRAJ20, or TRAV1-2/TRAJ12,
191 composes about 67 % of TCRα-detected cells in this cluster 0 (fig. S5E). Cluster 1 (activated: Act)
192 contained *TYMS*$^+$ proliferating cells and HLA-DR$^+$ activated cells. Compared to cluster 4 (memory
193 precursor: MP), cluster 5 expressed a lower level of CD127 and CCR7 and a higher level of *GZMK*
194 and CD279 (PD-1), consistent with the progenitor exhausted-like (PEX) phenotype described
195 previously (*31*). The clonality of these CD8$^+$ clusters showed that TD and PEX clusters contained
196 larger clones (fig. S5E), suggesting that these clusters underwent clonal expansion due to
197 activation. Notably, the cluster distribution of CD8$^+$ T cells differed between the two participants:
198 cluster TD2 and PEX were mainly present in ID2, while cluster TD1 was predominantly present
199 in ID27 (Fig. 6D).

200 To analyze the relationship between T-cell clones' kinetic profile and their phenotype in each T
201 cell clone, T cells in the first-, second, and long-term responder clones were extracted from the
202 dimensionality reduction plot of single-cell analysis. The second-responder clones mainly
203 belonged to the cluster Act. (90.7 % in ID2 and 90.2 % in ID27) (Fig. 6E and F). On the other
204 hand, the first-responder clones were predominantly composed of cluster TD2 (79.4% in ID2), and
205 very few belonged to cluster Act. Furthermore, we confirmed these relationships at the clonal level.
206 The heatmap of cluster distribution of CD8$^+$ clones exhibited that T cells in each clone were highly
207 skewed to one phenotype, suggesting that the differentiation stage of CD8$^+$ T cells was highly
208 synchronized in clones (Fig. 6G). Moreover, all second-responder clones skewed to cluster Act,
209 while the two first-responder clones skewed to cluster TD2 (Fig. 6G). These results suggested that
210 first-responders became terminally differentiated after the second dose, which led them to be
211 unresponsive and outcompeted by actively proliferating second-responders.

212 Then, we examined the phenotype of Spike-reactive clones. AIM$^+$ and AIM$^-$ T cell clones
213 determined in Fig. 4 and 5 were projected onto the dimensionality reduction plot, and their
214 distribution to clusters was compared. CD8$^+$ T cells of AIM clones were enriched in cluster Act in
215 participant ID2 and IL in ID27 (Fig. 6H and I). Moreover, we examined the phenotype of expanded
216 AIM+ clones with more than ten cells. At the clonal level, two AIM$^+$ clones skewed to cluster Act,

two clones skewed to IL, and the remaining three clones were a mixture of Act and other clusters (Fig. 6J). Interestingly, the two Act-skewed AIM$^+$ clones exhibited the second-responder pattern, while the frequency of the two IL-skewed AIM$^+$ clones remained stable at P2 and P3 (Fig. 6K). Although the number of expanded AIM$^+$ clones analyzed was small, these results indicate that Spike-reactive second-responder clones were actively proliferating after the second dose. In contrast, Spike-reactive clones with innate-like phenotypes were not responsive to mRNA vaccination.

Single-cell TCR analysis was also performed on CD4$^+$ T cells. Four clusters were identified in non-naive CD4$^+$ T cells; CCR7$^+$ CD62L$^+$ cluster 0 (central memory: CM), CD196 (CCR6)$^+$ CD127$^+$ cluster 1 (effector memory: EM), *IFNG*$^+$ HLA-DR$^+$ cluster 2 (activated: Act), and *FOXP3*$^+$ CD25$^+$ cluster 3 (regulatory T cells: Treg) (Fig. 7A-C and fig. S6A-C). The higher clonality of cluster 2 supported that this cluster underwent activation-induced clonal expansion (fig. S6D). Notably, T cells in AIM$^+$ clones were mainly composed of cells in the EM cluster and rarely contained cells in Act or Treg clusters, suggesting that the phenotype of AIM$^+$ CD4$^+$ T cells was more homogeneous than AIM$^+$ CD8$^+$ (Fig. 7D and E). We also attempted to analyze the relationship between the kinetics of CD4$^+$ T cell clones and their phenotypes. However, clear differences in cluster distribution between first-, second-, and long-term responders were not observed (Fig. 7F and G).

DISCUSSION

Through a longitudinal TCR repertoire analysis combined with an AIM assay using a Spike peptide pool, we demonstrated that the increase of Spike-reactive CD8$^+$ T cells following secondary vaccination was caused by second-responder clones, which replaced the first-responders. Moreover, single-cell analysis indicated that terminally differentiated first-responder clones were outcompeted by actively proliferating second-responders after the second vaccine dose. These results suggest that the vaccine-induced anti-Spike T-cell response was accompanied by clonal replacement of Spike-reactive T cells. These data are consistent with a dynamic turnover model of T-cell memory response under repetitive antigen challenges in humans receiving SARS-CoV-2 mRNA vaccinations (*14*).

There are several hypotheses to explain the mechanism underlying the clonal replacement of memory T cells following repetitive vaccination. One hypothesis is that first-responders are memory T cells cross-reactive to 'common cold' coronaviruses (CCCoV) that were present before the pandemic (pre-existing memory) (*32–35*). After the first dose, these pre-existing memory T cells might undergo a proliferative burst and differentiate into secondary memory with a weaker proliferation ability (*10*, *13*, *36*). Another possible mechanism is that the first-responders have high-affinity TCRs to Spike, compared to second-responders. Signals from the high-affinity TCRs of first-responders may induce greater expansion and effector differentiation after the first dose, resulting in reduced proliferative capacity to subsequent antigen exposure. A third possible mechanism is that second-responder clones are those that migrated into the vaccine-draining lymph node (dLN) relatively late during the primary response ("late-arriving" clones). Carton et al. demonstrated that late-arriving T cells divide less than early-arriving T cells during the first antigen challenge and their progeny proliferate more extensively during the second response (*37*). These possibilities could be addressed in future studies.

The strength of our dataset is that the sampling time point for bulk TCR repertoire analysis is uniform across the participants. As far as we know, this is the first report of longitudinal TCR

261 repertoire data before and after the mRNA vaccination with 41 participants, enabling the global
262 analysis of the kinetics of T-cell clones. Moreover, all participants reported no history of SARS-
263 CoV-2 infection (*15*). Thus, our data represent the exclusive effect of mRNA vaccination on T-
264 cell repertoire, although we can't exclude that some participants may have been asymptomatically
265 infected. Furthermore, we introduced the WGCNA (*16*) for the analysis of T-cell clones' kinetics,
266 originally used for the time-course transcriptional data to identify gene clusters associated with
267 biological events (*38*, *39*). Compared to the earlier methods for identifying expanded/contracted
268 clones between two time points (*40*, *41*), we believe that WGCNA identifies the kinetic patterns
269 of clones more flexibly.

270 To evaluate Spike-reactive T cell responses of the participants in our cohort, we integrated AIM
271 assays and TCR repertoire analyses. The AIM assay is widely used to evaluate the Spike-reactive
272 T cell responses (*5*, *21–23*). However, this assay underestimates the frequency of Spike-reactive
273 T cells compared to the use of peptide-major histocompatibility complex (pMHC) multimers (*2*).
274 The low sensitivity of the AIM assay may be because only a tiny proportion of Spike-reactive
275 clones become AIM^+, as suggested by fig. S3F. Thus, the inclusion of TCR sequencing can
276 improve the sensitivity of the AIM assay. Moreover, considering that the pMHC multimer assay
277 requires prior knowledge of participants' HLA allele, the AIM assay integrated with TCR
278 sequencing we performed in this study is a more suitable method to comprehensively detect
279 cellular immune response induced by mRNA vaccination. Through this approach, we identified
280 participants who exhibited a small number of AIM^+ second-responders, while the total amount of
281 second-responders was relatively high. For these participants, the epitopes recognized by Spike-
282 reactive clones may not have been efficiently presented on HLA from the Spike peptide pool used
283 in the AIM assay. Expanding the Spike peptide pool to cover a broader range of possible epitopes
284 may fill the gap between the total and AIM^+ second-responders in these participants.

285 One limitation in our study is the low sensitivity of the AIM assay. The frequency of AIM^+ $CD8^+$
286 T cells is reported to be as high as 1% of the non-naive fraction during the vaccination (*5*, *6*). To
287 collect a sufficient number (more than 100 cells) of cells for TCR sequencing, we defined AIM^+
288 $CD8^+$ T cells as expressing either CD137 or CD107a. However, this definition decreased the
289 specificity of AIM^+ $CD8^+$ clones compared to the analysis of $CD4^+$ clones. Moreover, performing
290 AIM assays at time points other than P3 (7 days after the second dose) is difficult because the AIM
291 positivity is lower than that in P3. Another limitation is the limited number of participants in whom
292 single-cell analysis was performed. Notably, the number of AIM^+ clones detected in the single-cell
293 analysis is too small to demonstrate the relationship between their response kinetics and
294 phenotypes after the second dose.

295 An important question is whether the clonal replacement we demonstrated in this study is specific
296 to the mRNA vaccination or is common to the other types of vaccination (peptide, inactivated
297 virus, etc.) or natural infections. We initially reported the dynamic turnover model through antigen
298 delivery systems using plasmid and viral vectors (*14*). In addition, in the case of yellow fever
299 vaccination, the responding $CD8^+$ clones are replaced between the prime and boost dose (*42*).
300 These observations suggest clonal replacement is a general phenomenon in establishing T-cell
301 memory through vaccination. It should also be noted that the current SARS-CoV-2 mRNA vaccine
302 strongly activates Spike-reactive $CD8^+$ T cells through the production of IFNα (*43*), which may
303 accelerate clonal replacement compared to other types of vaccination. Although the current study
304 analyzed only peripheral blood T cells, natural SARS-CoV-2 infection generates tissue-resident
305 memory T cells (TRM) in the lung (*44*). Considering that a subset of circulating effector T cells

have a higher capacity to form TRM (*45*), the replacement of pathogen reactive clones in blood after re-infection may be associated with the re-distribution of older clones from the blood to peripheral tissues and their differentiation to TRM. Moreover, it is unknown whether these TRM clones are also replaced under re-infection or continue to function as a defense against re-infection. Collectively, a systemic analysis of peripheral tissues and blood is necessary to understand the clonal replacement by natural infection.

As of August 2022, many countries implemented the third dose of mRNA vaccination, and several countries, including Japan, started offering fourth-dose vaccines for healthcare workers and the elderly. The third- and fourth- vaccination induces a more robust humoral and cellular immune response to SARS-CoV-2 (*46*, *47*), and increases the protection against SARS-CoV-2 infection, including the Omicron variant (*48*, *49*). However, considering the maintenance of memory T-cell populations by clonal replacement, which requires the mobilization of new clones, memory populations may eventually become unsustainable after repetitive vaccination, especially in elderly participants whose naive T-cell repertoire is decreased. Thus, the sustainability of clonal replacement under repetitive vaccination needs to be verified based on the participants' age and proportion of naive T cells in the future study. We believe that the comprehensive analysis of T cell clones like this study will provide the immunological basis for optimizing the strategy for mRNA vaccination.

In summary, we demonstrated the replacement of memory T-cell clones during SARS-CoV-2 mRNA vaccination. In contrast to humoral immunity mediated by memory B cells and long-lived plasma cells, where the memory response to the first viral variant encountered in childhood is preferentially employed even after the challenge of other variants in adults (original antigenic sin) (*50*, *51*), T cells appear to be able to replace memory population after repetitive challenges. This "re-writability" of T cell immunological memory enables them to effectively generate responses to variant strains of the virus.

MATERIALS AND METHODS

Study Design

Forty-one healthcare workers (≥20 years old) at Nara Medical University in Japan who had received the Pfizer-BNT162b2 vaccine between 10 March and 30 March 2021 were invited to participate as volunteers in the study. The Nara Medical University Ethics Committee approved the study (No. 3168). All study participants provided written informed consent. All participants had no history of suspected clinical SARS-CoV-2 infection. Peripheral blood samples were collected before receiving the first dose (P1), 1 week after receiving the first dose (P2), then 1 week (P3), 1 month (P4), 3 months, and 6 months after receiving the second dose. PBMCs were isolated from whole blood with BD vacutainer CPT tubes (BD), resuspended in CELLBANKER 1 (Takara), and stored at -80°C. The detailed study design was described in Kitabatake et al. (*15*).

Evaluation of anti-SARS-CoV-2 antibodies

All serum samples from vaccinated participants were tested for anti-RBD antibodies with a COVID-19 human IgG enzyme-linked immunosorbent assay kit per the manufacturer's instructions (RayBiotech Life, Inc. Peachtree Corners, GA, USA).

T-cell isolation from PBMCs

$CD4^+$ and $CD8^+$ T cells were magnetically isolated from PBMC. PBMC were thawed by warming frozen cryovials in a 37°C water bath. Cells were stained for 20 minutes at 4°C with 1st antibody

349 mix; Human TruStain FcX (BioLegend), anti-CD3-Pacific Blue (clone SK7, BioLegend), anti-
350 CD4-PE (clone SK3, BioLegend), anti-CD8-APC (clone SK1, BioLegend), and anti-CD19-APC
351 (clone HIB19, BD Biosciences). After washing with MACS buffer [0.5% BSA (Nacalai Tesque
352 Inc.), 2 mmol/L EDTA (Nacalai Tesque Inc.) in PBS (Nacalai Tesque Inc.)], Cells were stained
353 for 20 minutes at 4°C with 2nd antibody mix; BD IMag anti-PE Magnetic Particles-DM (Clone
354 E31-1459, BD) and anti-APC-Biotin (clone APC003, BioLegend). Then, the cell suspension was
355 diluted with MACS buffer and set on a magnet plate (DynaMag96SideSkirted) (Thermo Fisher
356 Scientific). The positive fraction was collected as CD4$^+$ T cells. The negative fraction was stained
357 with BD IMag Streptavidin Particles Plus-DM (BD) for 20 minutes at 4°C. Then, the cell
358 suspension was diluted with MACS buffer and set on a magnet plate. The positive fraction was
359 collected as CD8$^+$ T cells and B cells. The counts of CD4$^+$ T cells, CD8$^+$ T cells, and B cells were
360 determined using Flow-Count fluorospheres (Beckman) and a Cytoflex flow cytometer (Beckman).

361 **AIM assay and sorting Spike-reactive T cells.**

362 AIM assay was performed on P3 PBMC samples of 15 participants with varying levels of anti-
363 RBD antibody (Table S1). PBMC were thawed by warming frozen cryovials in a 37°C water bath
364 and resuspended in 10mL of in Culture Medium (CM) [10% fetal bovine serum (MP Bio Japan),
365 1% HEPES (Nakarai) and 1% penicillin/streptomycin (Nakarai) in RPMI-1640 medium (Nakarai)].
366 Cells were resuspended in 1mL of CM, then plated in 24-well plates and incubated overnight
367 (about 16 hours) in an incubator at 37°C, with 5% CO2. After incubation, cells were then
368 stimulated for 24 hours in stimulation medium [BD FastImmune CD28/CD49d Costimulatory
369 Reagent (final x100, BD Biosciences) and anti-human CD40 (final concentration of 0.5μg/mL,
370 clone HB14, BioLegend) in CM] with or without PepTivator SARS-CoV-2 Prot_S Complete (final
371 concentration of 1 mg/mL, Miltenyi). 20 hours post-stimulation, an anti-CD107a-FITC antibody
372 (final concentration of 5μg/mL, clone H4A3, BioLegend) was added to the culture. After four
373 hours, cells were washed in PBS supplemented with 10% FBS (10% FBS/PBS). Cells were stained
374 for 20 minutes at 4°C with antibody mix against CD4 (clone SK3, BioLegend), CD8 (clone RPA-
375 T8, BioLegend), CD14 (clone 63D3, BioLegend), CD19 (clone HIB19, BioLegend), CD45RA
376 (clone HI100, BioLegend), CD27 (clone O323, BioLegend), CD40L (clone 24-31, BioLegend),
377 CD69 (clone FN50) and CD137 (clone 4B4-1, BD). Cells were washed once in 10% FBS/PBS.
378 AIM$^+$ non-naïve CD4$^+$, AIM$^-$ non-naïve CD4$^+$, AIM$^+$ non-naïve CD8$^+$, and AIM$^-$ non-naive CD8$^+$
379 cells were sorted using FACS Aria II or Aria III (BD Biosciences). AIM$^+$ CD4$^+$ T cells were
380 defined by dual-expression of CD69 and CD40L. AIM$^+$ CD8$^+$ T cells were defined by expression
381 of either CD107a or CD137. Nonviable cells were excluded from the analysis based on forward
382 and side scatter profiles and propidium iodide staining. Data were analyzed using FlowJo software
383 (version 10.8.1; BD Biosciences).

384 **Sample preparation for single-cell analysis**

385 PBMC were thawed as described above, and 2x10^6 cells per sample were used for single-cell
386 analysis. 2x AbSeq master mix of Immune Discovery Panel (BD Biosciences) prepared as the
387 provider's protocol. Cells were resuspended with Cell Staining Buffer (BioLegend) supplemented
388 with Human TruStain FcX (BioLegend). After 2-3 minutes, the cell suspension was added with 2x
389 AbSeq master mix and stained for 15 minutes on ice. Then, the antibody mix for cell sorting was
390 added to the cell suspension and left on ice for 15 minutes for staining. Antibody mix for cell
391 sorting contained following antibodies; anti-CD3 (clone SK7, BioLegend), CD4 (clone SK3,
392 BioLegend), CD8 (clone SK1, BioLegend), CD14 (clone 63D3, BioLegend), CD19 (clone HIB19,
393 BioLegend), CD45RA (clone HI100, BioLegend), and CD27 (clone O323, BioLegend). Stained

394 cells were washed with Cell Staining Buffer. Then non-naive $CD4^+$ and $CD8^+$ cells were sorted
395 using FACS Aria II or Aria III (BD Biosciences). Data were analyzed using FlowJo software
396 (version 10.8.1; BD Biosciences).

397 **Library preparation and sequencing for TCR repertoire analysis**

398 TCR sequencing libraries for next-generation sequencing were prepared according to the
399 previous report (*52*). In brief, mRNA in T-cell lysate was captured by 10 µL of oligo-dT
400 immobilized Dynabeads M270 streptavidin (Thermo Fisher Scientific). mRNA-trapped beads
401 were suspended in 10 µL of RT mix and incubated for 60 min at 42ºC to perform reverse
402 transcription (RT) and template-switching. The composition of the RT mix was as follows; 1×
403 First Strand buffer (Thermo Fisher Scientific), 1 mM dNTP (Roche), 2.5 mM DTT (Thermo
404 Fisher Scientific), 1 M betaine (Sigma-Aldrich), 9 mM MgCl2 (NIPPON GENE), 1 U/µL
405 RNaseIn Plus RNase Inhibitor (Promega), 10 U/µL Superscript II (Thermo Fisher Scientific),
406 and 1 µM of trP1-TSO. To amplify the TCR cDNA containing complementarity determining
407 region 3 (CDR3), nested PCR of the TCR locus was performed, followed by the purification of
408 PCR product using an AM Pure XP kit (Beckman Coulter) at a 0.7:1 beads-to-sample ratio. The
409 third PCR was performed to amplify TCR libraries and add adaptor sequences for the next-
410 generation sequencer. The third-PCR products were purified as second PCR. Final TCR libraries,
411 whose lengths were about 600 base pairs, were sequenced using an Illumina Novaseq 6000 S4
412 flowcell (67 bp read 1 and 140 bp read 2) (Illumina). Only read2 contained the sequence
413 regarding the definition of T-cell clones. Oligonucleotides used and conditions for PCR reaction
414 and purification for library preparation were summarized in Table S2 and S3, respectively.

415 **Library preparation and sequencing for single-cell analysis**

416 Live cells were stained with Calcein AM (Nacalai) and counted using Flow-Count fluorospheres
417 (Beckman) and a Cytoflex flow cytometer. About 25,000 - 30,000 labeled cells were trapped and
418 reverse-transcribed using the BD Rhapsody™ (BD Biosciences), Targeted mRNA, and AbSeq
419 Amplification Kit (BD Biosciences), and Immune Response Panel HS (BD Biosciences) according
420 to the manufacturer's instructions. Targeted mRNA, TCRseq, and Abseq Index libraries were
421 prepared according to the manufacturer's instructions with the following modifications. (1) We
422 used the original set of primers for TCR amplification, as summarized in Table S2. (2) We
423 performed additional PCRs to introduce a unique dual index for sequencing (3rd PCR for mRNA
424 and TCR) or to enrich the desired product (5th PCR). (3) We used AMPure XP (Beckman-Coulter)
425 or ProNex Size-Selection DNA purification System (Promega) for the purification of PCR
426 products, as summarized in Table S4. Amplified libraries were quantified using a KAPA SYBR
427 Fast qPCR Kit (KAPA Biosystems), and size distribution was analyzed by Microchip
428 Electrophoresis System MultiNA (Shimadzu). Targeted RNAseq, TCRseq, and AbSeq libraries
429 were sequenced on an Illumina Novaseq 6000 S4 flowcell (67 bp read 1 and 140 bp read 2)
430 (Illumina) to a depth of approximately 20,000 reads, 7,000 reads, and 10,000 reads per cell,
431 respectively.

432 **Data processing of TCR sequencing reads**

433 Data processing of TCRseq was performed as previously reported (*52*). Briefly, Adapter
434 trimming and quality filtering of sequencing data were performed using Cutadapt-3.2 (*53*) and
435 PRINSEQ-0.20.4 (*54*). Sequencing data were processed by MiXCR-3.0.5 (*55*). In MiXCR,
436 filtered reads were aligned to reference mouse TCR V/D/J sequences registered in the
437 international ImMunoGeneTics (IMGT) information system. The Variable (V) and Joining (J)

segments of TCRs were represented in IMGT gene nomenclature. T-cell clones were determined as TCR reads with the same TCR V segment, J segment, and CDR3 nucleotide sequence.

For bulk TCRseq data, we regarded the $CD4^+$-$CD8^+$ overlapping clones in the same participant as contamination during T-cell isolation from PBMC because $CD4^+$ and $CD8^+$ T-cell repertoire are mutually exclusive (*56*). Thus, these overlapping clones were categorized into either $CD4^+$ or $CD8^+$ according to their dominance in $CD4^+$ and $CD8^+$ repertoire using VDJtools-1.2.1 (*57*). The sequencing reads of the sample were normalized to the cell count (bulk TCR sequencing data) or 16 times the cell count (AIM assay-TCRseq data) in each sample by the "DownSample" command of VDJtools-1.2.1 (*57*). For AIM assay-TCRseq data, TCR clones with 15 or fewer reads were regarded as sampling noise and removed from the dataset (*56*). The processed data have been deposited at the NCBI GEO; accession GSE210227 and GSE210228.

Grouping T-cell clones based on their kinetic profile using WGCNA

To identify the pattern of clones' kinetic profile, we performed WGCNA (*16*) on the top 150 clones detected at all four time points for each participant (Fig. 1B). First, the correlation network of kinetics profile of these selected clones (150 clones x 41 participants) was generated, and modules consisting of highly correlated clones were identified. We identified six and five modules by WGCNA for $CD8^+$ or $CD4^+$ repertoire, respectively. Next, the module's eigenvector, the first principal component of the kinetic profile of clones in the module, was calculated. Components of the eigenvectors were the standardized frequency at each time point. Then, the kinetics patterns were defined as the eigenvectors or inverted eigenvectors (multiplied by -1) of modules identified (Fig. 1C and fig. S1D).

We classified the clones detected at least two time points into one of these kinetics patterns. The criteria for assigning a clone to a particular kinetic pattern were the followings; the correlation coefficient between the kinetic pattern and the clone's kinetic profile was (1) higher than 0.85 and (2) higher than that between other kinetic patterns. Clones that did not meet these criteria for kinetic patterns were regarded as "unassigned."

Searching TCRs with reported Spike-reactivity using tcrdist3

To search previously reported SARS-Co-2 reactive TCRs in our dataset, we utilized the framework introduced in Mayer-Blackwell's study (*20*). In this framework, we first formed meta-clonotypes of public CoV-2-reactive TCRs (groups of TCRs that were biochemically similar). Then we searched TCRs conformant to the definition of the meta-clonotypes (meta-clonotype conformant TCRs).

Public CoV-2-reactive TCRs were curated from the three datasets (*17–19*). Francis's and Minervina's datasets were obtained by sorting SARS-CoV-2 antigen peptide-MHC multimer positive cells followed by single-cell TCR sequencing. Snyder's dataset was obtained by antigen stimulation following TCR sequencing (MIRA assay) (*58*). For Francis and Minervina's dataset, public CoV-2-reactive TCRs were grouped by their epitopes, then meta-clonotypes were formed for each group using tcrdist3, according to their instruction. In forming meta-clonotypes, optimal radii were estimated at which background TCRs were detected at a frequency of $< 10^{-6}$. In addition, for Snyder's dataset, the meta-clonotypes reported in Meyer-Blackwell's study were used.

We defined meta-clonotype conformant TCRs as TCRs that met the criteria of meta-clonotype defined by an optimized radius and the CDR3 motif constraint. Meta-clonotype conformant TCRs were searched using Snyder's, Francis's, and Minervina's datasets independently, then assigned

with the type of SARS-CoV-2 antigen corresponding to the meta-clonotypes ("Spike," "Membrane," etc.). If the assigned antigen types were inconsistent between datasets, the assignment based on Francis's and Minervina's datasets were adopted because these datasets were generated by sorting SARS-CoV-2 reactive T cells using peptide-MHC tetramer.

Defining Spike-reactive TCRs using TCRseq data from the AIM assay

We detected Spike-reactive clones using the dataset of AIM-assay TCRseq as in Fig. 4B. T-cell clones detected only in the AIM^+ repertoire were regarded as Spike-reactive clones. For T-cell clones detected in AIM+ and AIM^- repertoire, we calculated the "AIM+ enrichment ratio" for each clone by the following equation;

$$AIM\ enrichment\ ratio\ of\ clone\ X = \frac{AIM^+\ cell\ count\ in\ clone\ X / AIM^-\ cell\ count\ in\ clone\ X}{Total\ AIM^+\ cell\ count / Total\ AIM^-\ cell\ count},$$

where total AIM+ and AIM^- cell count were the count of sorted cells in AIM assay, and AIM^+ and AIM^- cell count in clone X were calculated as the value obtained by multiplying total cell count and clone's frequency in AIM^+ or AIM^- repertoire. Then, clones with an AIM^+ enrichment ratio over 4 were also defined as Spike-reactive clones.

Data processing of scRNAseq reads

Data processing of scRNAseq reads was performed as described in Shichino et al. (*59*). Adapter trimming of sequencing data was performed by using cutadapt 3.4 (*53*). Filtered reads were chunked into 16 parts for parallel processing using Seqkit 0.15.0 (*60*). Filtered cell barcode reads were annotated by Python script provided by BD with minor modifications to be compatible with Python3.8. Associated cDNA reads were mapped to reference RNA (build GRCh38 release-104) using bowtie2-2.4.2 (*61*) by the following parameters: -p 2 -D 20 -R 3 -N 0 -L 8 -I S,1,0.75 –norc –seed 656565 –reorder. Then, cell barcode information of each read was added to the bowtie2-mapped BAM files, and read counts of each gene in each cell barcode were counted by using mawk. Resulted count data was converted to genes x cells matrix file, and the knee-plot inflection threshold was detected using the DropletUtils package in R version 4.1.2 (*62*). In addition, we further estimate background beads using the emptyDrops formula in the DropletUtils package. Cells of total read count over inflection point were considered valid cells.

Data processing of AbSeq reads

For AbSeq data, adapter trimming of sequencing data was performed using cutadapt 3.4 (*53*). Filtered reads were chunked into 64 parts for parallel processing using Seqkit 0.15.0 (*60*). Filtered cell barcode reads were annotated by Python script provided by BD with minor modifications to be compatible with Python3.8. Associated AbSeq reads were mapped to known barcode fasta by using bowtie2-2.4.2 (*61*) by the following parameters: -p 2 -D 20 -R 3 -N 0 -L 8 -I S,1,0.75 –norc –seed 656565 –reorder–trim-to 3:39 –score-min L,-9,0 –mp 3,3 –np 3 –rdg 3,3. Then, cell barcode information of each read was added to the bowtie2-mapped BAM files, and read counts of each AbSeq tag in each cell barcode were counted using mawk. Resulted count data were converted to tags x cells matrix file by using the data.table package in R version 4.1.2, and top 1M cell barcodes were extracted.

scRNAseq/AbSeq data analysis

scRNAseq/AbSeq data analysis was performed using the R software package Seurat v4.0.1 (*24*). Expression data of targeted panel genes and surface proteins were converted to the Seurat object.

522 $CD4^+$ $CD8^-$ and $CD4^-$ $CD8^+$ cells were extracted based on the expression level of CD4 and CD8
523 proteins determined by AbSeq, as fig. S5A. Then, expression data was log-normalized and scaled
524 using NormalizeData and ScaleData function, respectively. For scRNAseq data, principal
525 component analysis (PCA) against all genes in the target panel was performed using RunPCA
526 (number of calculated principal components (PCs) was 100). Then, the enrichment of each PC was
527 calculated using the JackStraw and ScoreJackStraw function (num.replicate = 100), and PCs that
528 were significantly enriched ($p \leq 0.05$) were selected for further analysis. For AbSeq data, PCA
529 against all genes included in Immune Discovery Panel was performed using RunPCA, and the
530 same number of PCs as scRNAseq was selected for further analysis. Cell clustering was performed
531 based on the weighted-nearest neighbor graph using FindMultiModalNeighbors and FindClusters
532 against the significant PCs of scRNAseq and AbSeq (*24*). The dimensional reduction was
533 performed using RunUMAP based on the nearest neighbor graph determined by
534 FindMultiModalNeighbors. Marker genes of each identified cluster were identified using
535 FindAllMarkers function (test.use="Wilcox", min.pct=0.1, return.thresh=0.05). Clusters
536 constituted with contaminant cells determined by marker genes were excluded, and the above
537 analysis procedure was repeated.

538 **Data processing and analysis of scTCRseq**

539 Raw data of single-cell TCR sequencing were processed by pipeline produced by
540 ImmunoGeneTeqs, Inc., as described previously (*52*). Briefly, sequencing reads were separated by
541 cell barcode, then adapter trimming and quality filtering of sequencing data were performed using
542 cutadapt 3.4 (*53*). PCR and sequencing errors were corrected by lighter v1.1.2 (*63*) with the
543 following parameters: -newQual 25 -maxcor 4 -K 20. Error-corrected sequence reads were
544 processed by MiXCR (*55*) to generate the list of TCRα or TCRβ sequences for each cell barcode,
545 using reference mouse TCR V/D/J sequences registered in the international IMGT information
546 system. Quality filtering of cell barcodes was performed with the following criteria: (1) more than
547 32 TCR reads were detected. (2) the proportion of the most frequent TCR sequence in cell barcodes
548 was over 0.6. (3) the cell barcode was annotated to the T cell cluster in scRNAseq/AbSeq analysis.
549 Finally, the most frequent sequence of TCRα and TCRβ was adopted and paired in each cell
550 barcode. Identified TCRα or TCRβ sequence was imported into the meta.data matrix in Seurat
551 object of scRNAseq/AbSeq data based on the cellular barcode identities. T-cell clones were
552 determined as cells with the same TCRβ sequence defined by V segment, J segment, and CDR3
553 nucleotide sequence. The frequency of each clone was calculated as the proportion of cells
554 belonging to the clone in all T cells whose TCRβ sequence was assigned. The 1 - Pielou index was
555 used to evaluate the clonality of clusters, which was calculated as the following formula: $1 -$
556 $\sum_{i=1}^{n} p_i \log_e(p_i) / \log_e(n)$.

557 **Quantification and statistical analysis**

558 Statistical analyses were performed using GraphPad Prism (ver9.4.0) software (GraphPad
559 Software). Friedman test with Dunn's multiple comparisons test was run on the comparison
560 between time points or kinetic profile patterns. Friedman test with Dunn's multiple comparisons
561 test was run on the comparison between time points or kinetic profile patterns. Wilcoxon matched-
562 pairs signed rank test was run on the comparison between AIM^+ and AIM^- clones. Mann-Whitney
563 test was run on the comparison between AIM-high and AIM-low participants. Spearman
564 correlation test was run on the correlation analysis. Asterisks to indicate significance
565 corresponding to the following: ***P<0.001; **P<0.005; *P<0.05; n.s. non-significant (P≥0.05).

566

567 **Supplementary Materials**

568 Fig. S1 WGCNA for identifying patterns of clones' kinetic profile.

569 Fig. S2 Total frequency of kinetic profile patterns during vaccination.

570 Fig. S3 Identifying Spike-reactive clones by integrating TCR sequencing with AIM assay.

571 Fig. S4 Total frequency of Spike-reactive clones in each kinetic profile pattern during vaccination.

572 Fig. S5 Characterization of CD8+ T cell clusters observed in single-cell analysis.

573 Fig. S6 Characterization of CD4+ T cell clusters observed in single-cell analysis.

574 Table S1 List of participants on whom AIM assay was performed.

575 Table S2 Oligonucleotides list used in this study.

576 Table S3 Conditions for PCR reaction and purification for TCRseq library preparation.

577 Table S4 Conditions for PCR reaction and purification for scRNA/TCRseq library preparation.

578 Table S5 Antibody list used in this study.

579 Table S6 Reagent list used in this study.

580 Table S7 Algorithms used in this study.

581

582 **References and Notes**

583 1. X. Han, P. Xu, Q. Ye, Analysis of COVID-19 vaccines: Types, thoughts, and application.
584 *J. Clin. Lab. Anal.* **35**, 1–7 (2021).

585 2. U. Sahin, A. Muik, I. Vogler, E. Derhovanessian, L. M. Kranz, M. Vormehr, J. Quandt, N.
586 Bidmon, A. Ulges, A. Baum, K. E. Pascal, D. Maurus, S. Brachtendorf, V. Lörks, J.
587 Sikorski, P. Koch, R. Hilker, D. Becker, A. K. Eller, J. Grützner, M. Tonigold, C. Boesler,
588 C. Rosenbaum, L. Heesen, M. C. Kühnle, A. Poran, J. Z. Dong, U. Luxemburger, A.
589 Kemmer-Brück, D. Langer, M. Bexon, S. Bolte, T. Palanche, A. Schultz, S. Baumann, A.
590 J. Mahiny, G. Boros, J. Reinholz, G. T. Szabó, K. Karikó, P. Y. Shi, C. Fontes-Garfias, J.
591 L. Perez, M. Cutler, D. Cooper, C. A. Kyratsous, P. R. Dormitzer, K. U. Jansen, Ö.
592 Türeci, BNT162b2 vaccine induces neutralizing antibodies and poly-specific T cells in
593 humans. *Nature*. **595**, 572–577 (2021).

594 3. A. Pegu, S. E. O'Connell, S. D. Schmidt, S. O'Dell, C. A. Talana, L. Lai, J. Albert, E.
595 Anderson, H. Bennett, K. S. Corbett, B. Flach, L. Jackson, B. Leav, J. E. Ledgerwood, C.
596 J. Luke, M. Makowski, M. C. Nason, P. C. Roberts, M. Roederer, P. A. Rebolledo, C. A.
597 Rostad, N. G. Rouphael, W. Shi, L. Wang, A. T. Widge, E. S. Yang, J. H. Beigel, B. S.
598 Graham, J. R. Mascola, M. S. Suthar, A. B. McDermott, N. A. Doria-Rose, Durability of
599 mRNA-1273 vaccine-induced antibodies against SARS-CoV-2 variants. *Science (80-.).*
600 **373**, 1372–1377 (2021).

601 4. J. Mateus, J. M. Dan, Z. Zhang, C. R. Moderbacher, M. Lammers, B. Goodwin, A. Sette,
602 S. Crotty, D. Weiskopf, Low-dose mRNA-1273 COVID-19 vaccine generates durable
603 memory enhanced by cross-reactive T cells. *Science (80-.).* **374**, 1–18 (2021).

604 5. M. M. Painter, D. Mathew, R. R. Goel, S. A. Apostolidis, A. Pattekar, O. Kuthuru, A. E.
605 Baxter, R. S. Herati, D. A. Oldridge, S. Gouma, P. Hicks, S. Dysinger, K. A. Lundgreen,
606 L. Kuri-Cervantes, S. Adamski, A. Hicks, S. Korte, J. R. Giles, M. E. Weirick, C. M.
607 McAllister, J. Dougherty, S. Long, K. D'Andrea, J. T. Hamilton, M. R. Betts, P. Bates, S.
608 E. Hensley, A. Grifoni, D. Weiskopf, A. Sette, A. R. Greenplate, E. J. Wherry, Rapid
609 induction of antigen-specific CD4+ T cells is associated with coordinated humoral and
610 cellular immunity to SARS-CoV-2 mRNA vaccination. *Immunity*. **54**, 2133-2142.e3
611 (2021).

612 6. G. Guerrera, M. Picozza, S. D'Orso, R. Placido, M. Pirronello, A. Verdiani, A. Termine,
613 C. Fabrizio, F. Giannessi, M. Sambucci, M. P. Balice, C. Caltagirone, A. Salvia, A.
614 Rossini, L. Battistini, G. Borsellino, BNT162b2 vaccination induces durable SARS-CoV-
615 2–specific T cells with a stem cell memory phenotype. *Sci. Immunol.* **6**, 1–18 (2021).

616 7. P. Moss, The T cell immune response against SARS-CoV-2. *Nat. Immunol.* **23**, 186–193
617 (2022).

618 8. D. T. Skelly, A. C. Harding, J. Gilbert-Jaramillo, M. L. Knight, S. Longet, A. Brown, S.
619 Adele, E. Adland, H. Brown, S. Chinnakannan, T. Donnison, M. Ali, P. Rongkard, M.
620 Pace, P. Zacharopoulou, N. Robinson, A. Csala, C. De Lara, C. L. Hutchings, H. Mehta,
621 L. N. Lee, M. Edmans, C. P. Hackstein, P. Phalora, W. Li, E. Phillips, T. Malone, A.
622 Ogbe, C. Jay, T. Tipoe, T. Tipton, L. Stafford, A. J. Mentzer, S. A. Johnson, A. Amini, T.
623 Marjot, S. Dimitriadis, B. Simmons, A. Deeks, S. Kerneis, H. Abuelgasim, R. Wilson, S.
624 R. Thomas, A. Watson, A. Alhussni, J. Cutteridge, E. Weeks, L. Denly, K. Lillie, J.
625 Holmes, P. C. Matthews, D. O'Donnell, T. K. Tan, L. Schimanski, K. Y. A. Huang, P.
626 Rijal, L. Turtle, T. de Silva, A. Richter, C. J. A. Duncan, R. P. Payne, S. C. Moore, J. C.
627 Knight, M. P. Cassar, B. Raman, S. Neubauer, A. Fries, N. P. Talbot, N. Petousi, L. P. Ho,
628 Y. Peng, T. Dong, S. Camara, S. Marinou, A. Linder, S. Adlou, M. Kasanyinga, A.
629 Bridges-Webb, J. Hill, L. Silva-Reyes, L. Blackwell, J. Frater, P. Goulder, C. P. Conlon,
630 K. Jeffery, C. Dold, A. J. Pollard, A. Sigal, T. de Oliveira, A. R. Townsend, P. Klenerman,
631 S. J. Dunachie, E. Barnes, M. W. Carroll, W. S. James, Two doses of SARS-CoV-2
632 vaccination induce robust immune responses to emerging SARS-CoV-2 variants of
633 concern. *Nat. Commun.* **12**, 1–12 (2021).

634 9. D. L. Woodland, Jump-starting the immune system: Prime-boosting comes of age. *Trends*
635 *Immunol.* **25**, 98–104 (2004).

636 10. D. Masopust, S.-J. Ha, V. Vezys, R. Ahmed, Stimulation History Dictates Memory CD8 T
637 Cell Phenotype: Implications for Prime-Boost Vaccination. *J. Immunol.* **177**, 831–839
638 (2006).

639 11. V. Vezys, A. Yates, K. A. Casey, G. Lanier, R. Ahmed, R. Antia, D. Masopust, Memory
640 CD8 T-cell compartment grows in size with immunological experience. *Nature*. **457**, 196–
641 199 (2009).

642 12. K. A. Fraser, J. M. Schenkel, S. C. Jameson, V. Vezys, D. Masopust, Preexisting High
643 Frequencies of Memory CD8+ T Cells Favor Rapid Memory Differentiation and
644 Preservation of Proliferative Potential upon Boosting. *Immunity*. **39**, 171–183 (2013).

645 13. T. C. Wirth, H. H. Xue, D. Rai, J. T. Sabel, T. Bair, J. T. Harty, V. P. Badovinac,
646 Repetitive antigen stimulation induces stepwise transcriptome diversification but

preserves a core signature of memory CD8+ T cell differentiation. *Immunity*. **33**, 128–140 (2010).

14. M. Kurachi, K. Kakimi, S. Ueha, K. Matsushima, Maintenance of memory CD8+ T cell diversity and proliferative potential by a primary response upon re-challenge. *Int. Immunol.* **19**, 105–115 (2007).

15. M. Kitabatake, N. Ouji-Sageshima, S. Sonobe, R. Furukawa, M. Konda, A. Hara, H. Aoki, Y. Suzuki, N. Imakita, A. Nakano, Y. Fujita, S. Shichino, R. Nakano, S. Ueha, K. Kasahara, S. Muro, H. Yano, K. Matsushima, T. Ito, Transition of antibody titers after the SARS-CoV-2 mRNA vaccine in Japanese healthcare workers. *medRxiv*. 1-9, (2021). doi: https://doi.org/10.1101/2021.12.28.21268435.

16. P. Langfelder, S. Horvath, WGCNA: An R package for weighted correlation network analysis. *BMC Bioinformatics*. **9** (2008), doi:10.1186/1471-2105-9-559.

17. T. M. Snyder, R. M. Gittelman, M. Klinger, D. H. May, E. J. Osborne, H. J. Zahid, I. M. Kaplan, J. N. Dines, M. T. Noakes, R. Pandya, X. Chen, S. Elasady, E. Svejnoha, P. Ebert, M. W. Pesesky, P. De, H. O. Donnell, Q. Degottardi, G. Keitany, J. Lu, A. Vong, P. Fields, J. Greissl, L. Baldo, S. Semprini, C. Cerchione, O. M. Delmonte, K. Dobbs, G. Carreño-tarragona, S. Barrio, M. D. Angio, P. Bonfanti, M. F. Tompkins, C. Alba, C. Dalgard, J. Martinez-lopez, J. M. Carlson, H. S. Robins, Magnitude and Dynamics of the T-Cell Response to SARS-CoV-2 Infection at Both Individual and Population Levels. *medRxiv*. 1-33, (2020). doi: 10.1101/2020.07.31.20165647.

18. J. M. Francis, D. Leistritz-Edwards, A. Dunn, C. Tarr, J. Lehman, C. Dempsey, A. Hamel, V. Rayon, G. Liu, Y. Wang, M. Wille, M. Durkin, K. Hadley, A. Sheena, B. Roscoe, M. Ng, G. Rockwell, M. Manto, E. Gienger, J. Nickerson, MGH COVID-19 Collection and Processing Team2‡, A. Moarefi, M. Noble, T. Malia, P. D. Bardwell, W. Gordon, J. Swain, M. Skoberne, K. Sauer, T. Harris, A. W. Goldrath, A. K. Shalek, A. J. Coyle, C. Benoist, D. C. Pregibon, N. Jilg, J. Li, A. Rosenthal, C. Wong, G. Daley, D. Golan, H. Heller, A. Sharpe, B. A. Abayneh, P. Allen, D. Antille, K. Armstrong, S. Boyce, J. Braley, K. Branch, K. Broderick, J. Carney, A. Chan, S. Davidson, M. Dougan, D. Drew, A. Elliman, K. Flaherty, J. Flannery, P. Forde, E. Gettings, A. Griffin, S. Grimmel, K. Grinke, K. Hall, M. Healy, D. Henault, G. Holland, C. Kayitesi, V. LaValle, Y. Lu, S. Luthern, J. M. Schneider, B. Martino, R. McNamara, C. Nambu, S. Nelson, M. Noone, C. Ommerborn, L. C. Pacheco, N. Phan, F. A. Porto, E. Ryan, K. Selleck, S. Slaughenhaupt, K. S. Sheppard, E. Suschana, V. Wilson, M. Carrington, M. Martin, Y. Yuki, G. Alter, A. Balazs, J. Bals, M. Barbash, Y. Bartsch, J. Boucau, M. Carrington, J. Chevalier, F. Chowdhury, E. DeMers, K. Einkauf, J. Fallon, L. Fedirko, K. Finn, P. Garcia-Broncano, M. S. Ghebremichael, C. Hartana, C. Jiang, K. Judge, P. Kaplonek, M. Karpell, P. Lai, E. C. Lam, K. Lefteri, X. Lian, M. Lichterfeld, D. Lingwood, H. Liu, J. Liu, N. Ly, Z. M. Hill, A. Michell, I. Millstrom, N. Miranda, C. O'Callaghan, M. Osborn, S. Pillai, Y. Rassadkina, A. Reissis, F. Ruzicka, K. Seiger, L. Sessa, C. Sharr, S. Shin, N. Singh, W. Sun, X. Sun, H. Ticheli, A. Trocha-Piechocka, B. Walker, D. Worrall, X. G. Yu, A. Zhu, Allelic variation in class I HLA determines CD8+ T cell repertoire shape and cross-reactive memory responses to SARS-CoV-2. *Sci. Immunol.* **3070**, eabk3070 (2021).

19. A. A. Minervina, M. V. Pogorelyy, A. M. Kirk, J. C. Crawford, E. K. Allen, C. H. Chou, R. C. Mettelman, K. J. Allison, C. Y. Lin, D. C. Brice, X. Zhu, K. Vegesana, G. Wu, S.

691 Trivedi, P. Kottapalli, D. Darnell, S. McNeely, S. R. Olsen, S. Schultz-Cherry, J. H.
692 Estepp, A. Gaur, J. Hoffman, M. Mori, L. Tang, E. Tuomanen, R. Webby, H. Hakim, R.
693 T. Hayden, D. R. Hijano, R. Bajracharya, W. Awad, L. A. Van de Velde, B. L. Clark, T.
694 L. Wilson, A. Souquette, A. Castellaw, R. H. Dallas, J. Hodges, A. Gowen, J. Russell-
695 Bell, J. Sparks, D. E. Wittman, T. P. Fabrizio, S. Cherry, E. K. Roubidoux, V. Cortez, P.
696 Freiden, N. Wohlgemuth, K. Whitt, M. A. McGargill, J. Wolf, P. G. Thomas, SARS-CoV-
697 2 antigen exposure history shapes phenotypes and specificity of memory CD8+ T cells.
698 *Nat. Immunol.* **23**, 781–790 (2022).

699 20. K. Mayer-Blackwell, S. Schattgen, L. Cohen-Lavi, J. C. Crawford, A. Souquette, J. A.
700 Gaevert, T. Hertz, P. G. Thomas, P. G. Bradley, A. Fiore-Gartland, Tcr meta-clonotypes
701 for biomarker discovery with tcrdist3 enabled identification of public, hla-restricted
702 clusters of sars-cov-2 tcrs. *Elife*. **10**, 1–32 (2021).

703 21. M. R. Betts, J. M. Brenchley, D. A. Price, S. C. De Rosa, D. C. Douek, M. Roederer, R.
704 A. Koup, Sensitive and viable identification of antigen-specific CD8+ T cells by a flow
705 cytometric assay for degranulation. *J. Immunol. Methods*. **281**, 65–78 (2003).

706 22. S. Reiss, A. E. Baxter, K. M. Cirelli, J. M. Dan, A. Morou, A. Daigneault, N. Brassard, G.
707 Silvestri, J. P. Routy, C. Havenar-Daughton, S. Crotty, D. E. Kaufmann, Comparative
708 analysis of activation induced marker (AIM) assays for sensitive identification of antigen-
709 specific CD4 T cells. *PLoS One*. **12**, 1–22 (2017).

710 23. C. J. Thieme, M. Anft, K. Paniskaki, A. Blazquez-Navarro, A. Doevelaar, F. S. Seibert, B.
711 Hoelzer, M. J. Konik, M. M. Berger, T. Brenner, C. Tempfer, C. Watzl, T. L. Meister, S.
712 Pfaender, E. Steinmann, S. Dolff, U. Dittmer, T. H. Westhoff, O. Witzke, U. Stervbo, T.
713 Roch, N. Babel, Robust T Cell Response Toward Spike, Membrane, and Nucleocapsid
714 SARS-CoV-2 Proteins Is Not Associated with Recovery in Critical COVID-19 Patients.
715 *Cell Reports Med.* **1**, 100092 (2020).

716 24. Y. Hao, S. Hao, E. Andersen-Nissen, W. M. Mauck, S. Zheng, A. Butler, M. J. Lee, A. J.
717 Wilk, C. Darby, M. Zager, P. Hoffman, M. Stoeckius, E. Papalexi, E. P. Mimitou, J. Jain,
718 A. Srivastava, T. Stuart, L. M. Fleming, B. Yeung, A. J. Rogers, J. M. McElrath, C. A.
719 Blish, R. Gottardo, P. Smibert, R. Satija, Integrated analysis of multimodal single-cell
720 data. *Cell*. **184**, 3573-3587.e29 (2021).

721 25. F. Sallusto, D. Lenig, R. Förster, M. Lipp, A. Lanzavecchia, Two subsets of memory T
722 lymphocytes with distinct homing potentials and effector functions. *Nature*. **401**, 708–712
723 (1999).

724 26. D. Hamann, P. A. Baars, M. H. G. Rep, B. Hooibrink, S. R. Kerkhof-Garde, M. R. Klein,
725 R. A. W. Van Lier, Phenotypic and functional separation of memory and effector human
726 CD8+ T cells. *J. Exp. Med.* **186**, 1407–1418 (1997).

727 27. M. Dusseaux, E. Martin, N. Serriari, I. Péguillet, V. Premel, D. Louis, M. Milder, L. L.
728 Bourhis, C. Soudais, E. Treiner, O. Lantz, Human MAIT cells are xenobiotic-resistant,
729 tissue-targeted, CD161hi IL-17–secreting T cells. Blood. 117(4), 1250-1259 (2011). doi:
730 10.1182/blood-2010-08-303339.

731 28. C. Zheng, L. Zheng, J. K. Yoo, H. Guo, Y. Zhang, X. Guo, B. Kang, R. Hu, J. Y. Huang,
732 Q. Zhang, Z. Liu, M. Dong, X. Hu, W. Ouyang, J. Peng, Z. Zhang, Landscape of

733 Infiltrating T Cells in Liver Cancer Revealed by Single-Cell Sequencing. *Cell*. **169**, 1342-
734 1356.e16 (2017).

735 29. A. Kurioka, L. J. Walker, P. Klenerman, C. B. Willberg, MAIT cells: new guardians of
736 the liver. *Clin. Transl. Immunol.* **5**, e98 (2016).

737 30. M. Lepore, A. Kalinicenko, A. Colone, B. Paleja, A. Singhal, A. Tschumi, B. Lee, M.
738 Poidinger, F. Zolezzi, L. Quagliata, P. Sander, E. Newell, A. Bertoletti, L. Terracciano, G.
739 De Libero, L. Mori, Parallel T-cell cloning and deep sequencing of human MAIT cells
740 reveal stable oligoclonal TCRβ 2 repertoire. *Nat. Commun.* **5** (2014),
741 doi:10.1038/ncomms4866.

742 31. G. Galletti, G. De Simone, E. M. C. Mazza, S. Puccio, C. Mezzanotte, T. M. Bi, A. N.
743 Davydov, M. Metsger, E. Scamardella, G. Alvisi, F. De Paoli, V. Zanon, A. Scarpa, B.
744 Camisa, F. S. Colombo, A. Anselmo, C. Peano, S. Polletti, D. Mavilio, L. Gattinoni, S. K.
745 Boi, B. A. Youngblood, R. E. Jones, D. M. Baird, E. Gostick, S. Llewellyn-Lacey, K.
746 Ladell, D. A. Price, D. M. Chudakov, E. W. Newell, M. Casucci, E. Lugli, Two subsets of
747 stem-like CD8+ memory T cell progenitors with distinct fate commitments in humans.
748 *Nat. Immunol.* **21**, 1552–1562 (2020).

749 32. A. Sette, S. Crotty, Pre-existing immunity to SARS-CoV-2: the knowns and unknowns.
750 *Nat. Rev. Immunol.* **20**, 457–458 (2020).

751 33. A. Grifoni, D. Weiskopf, S. I. Ramirez, J. Mateus, J. M. Dan, C. R. Moderbacher, S. A.
752 Rawlings, A. Sutherland, L. Premkumar, R. S. Jadi, D. Marrama, A. M. de Silva, A.
753 Frazier, A. F. Carlin, J. A. Greenbaum, B. Peters, F. Krammer, D. M. Smith, S. Crotty, A.
754 Sette, Targets of T Cell Responses to SARS-CoV-2 Coronavirus in Humans with COVID-
755 19 Disease and Unexposed Individuals. *Cell*. **181**, 1489-1501.e15 (2020).

756 34. D. Weiskopf, K. S. Schmitz, M. P. Raadsen, A. Grifoni, N. M. A. Okba, H. Endeman, J.
757 P. C. van den Akker, R. Molenkamp, M. P. G. Koopmans, E. C. M. van Gorp, B. L.
758 Haagmans, R. L. de Swart, A. Sette, R. D. de Vries, Phenotype and kinetics of SARS-
759 CoV-2-specific T cells in COVID-19 patients with acute respiratory distress syndrome.
760 *Sci. Immunol.* **5**, 1–11 (2020).

761 35. P. Bacher, E. Rosati, D. Esser, G. R. Martini, C. Saggau, E. Schiminsky, J. Dargvainiene,
762 I. Schröder, I. Wieters, Y. Khodamoradi, F. Eberhardt, M. J. G. T. Vehreschild, H. Neb,
763 M. Sonntagbauer, C. Conrad, F. Tran, P. Rosenstiel, R. Markewitz, K. P. Wandinger, M.
764 Augustin, J. Rybniker, M. Kochanek, F. Leypoldt, O. A. Cornely, P. Koehler, A. Franke,
765 A. Scheffold, Low-Avidity CD4+ T Cell Responses to SARS-CoV-2 in Unexposed
766 Individuals and Humans with Severe COVID-19. *Immunity*. **53**, 1258-1271.e5 (2020).

767 36. H. Kay Chung, B. McDonald, S. M. Kaech, The architectural design of CD8+ T cell
768 responses in acute and chronic infection: Parallel structures with divergent fates. *J. Exp.*
769 *Med.* **218**, 1–15 (2021).

770 37. D. M. Catron, L. K. Rusch, J. Hataye, A. A. Itano, M. K. Jenkins, CD4+ T cells that enter
771 the draining lymph nodes after antigen injection participate in the primary response and
772 become central-memory cells. *J. Exp. Med.* **203**, 1045–1054 (2006).

773 38. S. Shichino, S. Ueha, S. Hashimoto, M. Otsuji, J. Abe, T. Tsukui, S. Deshimaru, T.
774 Nakajima, M. Kosugi-Kanaya, F. H. W. Shand, Y. Inagaki, H. Shimano, K. Matsushima,

775 Transcriptome network analysis identifies protective role of the LXR/SREBP-1c axis in
776 murine pulmonary fibrosis. *JCI Insight*. **4** (2019), doi:10.1172/jci.insight.122163.

777 39. T. A. Doering, A. Crawford, J. M. Angelosanto, M. A. Paley, C. G. Ziegler, E. J. Wherry,
778 Network Analysis Reveals Centrally Connected Genes and Pathways Involved in CD8+ T
779 Cell Exhaustion versus Memory. *Immunity*. **37**, 1130–1144 (2012).

780 40. J. Rytlewski, S. Deng, T. Xie, C. Davis, H. Robins, E. Yusko, J. Bienkowska, Model to
781 improve specificity for identification of clinically-relevant expanded T cells in peripheral
782 blood. *PLoS One*. **14**, 1–10 (2019).

783 41. W. S. DeWitt, R. O. Emerson, P. Lindau, M. Vignali, T. M. Snyder, C. Desmarais, C.
784 Sanders, H. Utsugi, E. H. Warren, J. McElrath, K. W. Makar, A. Wald, H. S. Robins,
785 Dynamics of the Cytotoxic T Cell Response to a Model of Acute Viral Infection. *J. Virol.*
786 **89**, 4517–4526 (2015).

787 42. A. A. Minervina, M. V. Pogorelyy, E. A. Komech, V. K. Karnaukhov, P. Bacher, E.
788 Rosati, A. Franke, D. M. Chudakov, I. Z. Mamedov, Y. B. Lebedev, T. Mora, A. M.
789 Walczak, Primary and secondary anti-viral response captured by the dynamics and
790 phenotype of individual T cell clones. *Elife*. **9**, 1–21 (2020).

791 43. C. Li, A. Lee, L. Grigoryan, P. S. Arunachalam, M. K. D. Scott, M. Trisal, F. Wimmers,
792 M. Sanyal, P. A. Weidenbacher, Y. Feng, J. Z. Adamska, E. Valore, Y. Wang, R. Verma,
793 N. Reis, D. Dunham, R. O'Hara, H. Park, W. Luo, A. D. Gitlin, P. Kim, P. Khatri, K. C.
794 Nadeau, B. Pulendran, Mechanisms of innate and adaptive immunity to the Pfizer-
795 BioNTech BNT162b2 vaccine. *Nat. Immunol.* **23**, 543–555 (2022).

796 44. M. M. L. Poon, K. Rybkina, Y. Kato, M. Kubota, R. Matsumoto, N. I. Bloom, Z. Zhang,
797 K. M. Hastie, A. Grifoni, D. Weiskopf, S. B. Wells, B. B. Ural, N. Lam, P. A. Szabo, P.
798 Dogra, Y. S. Lee, J. I. Gray, M. C. Bradley, M. A. Brusko, T. M. Brusko, E. O. Saphire,
799 T. J. Connors, A. Sette, S. Crotty, D. L. Farber, SARS-CoV-2 infection generates tissue-
800 localized immunological memory in humans. *Sci. Immunol.* **6** (2021),
801 doi:10.1126/sciimmunol.abl9105.

802 45. L. Kok, F. E. Dijkgraaf, J. Urbanus, K. Bresser, D. W. Vredevoogd, R. F. Cardoso, L.
803 Perié, J. B. Beltman, T. N. Schumacher, A committed tissue-resident memory T cell
804 precursor within the circulating CD8+ effector T cell pool. *J. Exp. Med.* **217** (2020),
805 doi:10.1084/JEM.20191711.

806 46. Y. Lustig, T. Gonen, L. Meltzer, M. Gilboa, V. Indenbaum, C. Cohen, S. Amit, H. Jaber,
807 R. Doolman, K. Asraf, C. Rubin, R. Fluss, E. Mendelson, L. Freedman, G. Regev-
808 Yochay, Y. Kreiss, Superior immunogenicity and effectiveness of the third compared to
809 the second BNT162b2 vaccine dose. *Nat. Immunol.* **23**, 940–946 (2022).

810 47. A. P. S. Munro, S. Feng, L. Janani, V. Cornelius, P. K. Aley, G. Babbage, D. Baxter, M.
811 Bula, K. Cathie, K. Chatterjee, K. Dodd, Y. Enever, E. Qureshi, A. L. Goodman, C. A.
812 Green, L. Harndahl, J. Haughney, A. Hicks, A. A. van der Klaauw, N. Kanji, V. Libri, M.
813 J. Llewelyn, A. C. McGregor, M. Maallah, A. M. Minassian, P. Moore, M. Mughal, Y. F.
814 Mujadidi, K. Holliday, O. Osanlou, R. Osanlou, D. R. Owens, M. Pacurar, A. Palfreeman,
815 D. Pan, T. Rampling, K. Regan, S. Saich, T. Bawa, D. Saralaya, S. Sharma, R. Sheridan,
816 E. C. Thomson, S. Todd, C. Twelves, R. C. Read, S. Charlton, B. Hallis, M. Ramsay, N.
817 Andrews, T. Lambe, J. S. Nguyen-Van-Tam, M. D. Snape, X. Liu, S. N. Faust, A. P. S.

Munro, S. Feng, L. Janani, V. Cornelius, P. K. Aley, G. Babbage, D. Baxter, M. Bula, K. Cathie, K. Chatterjee, K. Dodd, Y. Enever, E. Qureshi, A. L. Goodman, C. A. Green, L. Harndahl, J. Haughney, A. Hicks, A. A. van der Klaauw, N. Kanji, V. Libri, M. J. Llewelyn, A. C. McGregor, A. M. Minassian, P. Moore, M. Mughal, Y. F. Mujadidi, K. Holliday, O. Osanlou, R. Osanlou, D. R. Owens, M. Pacurar, A. Palfreeman, D. Pan, T. Rampling, K. Regan, S. Saich, T. Bawa, D. Saralaya, S. Sharma, R. Sheridan, M. Maallah, E. C. Thomson, S. Todd, C. Twelves, R. C. Read, S. Charlton, B. Hallis, M. Ramsay, N. Andrews, T. Lambe, J. S. Nguyen-Van-Tam, M. D. Snape, X. Liu, S. N. Faust, A. Riordan, A. Ustianowski, C. Rogers, K. Katechia, A. Cooper, A. Freedman, R. Hughes, L. Grundy, L. Tudor Jones, E. Harrison, E. Snashall, L. Mallon, K. Burton, K. Storton, M. Munusamy, B. Tandy, A. Egbo, S. Cox, N. N. Ahmed, A. Shenoy, R. Bousfield, D. Wixted, H. Gutteridge, B. Mansfield, C. Herbert, J. Murira, J. Calderwood, D. Barker, J. Brandon, H. Tulloch, S. Colquhoun, H. Thorp, H. Radford, J. Evans, H. Baker, J. Thorpe, S. Batham, J. Hailstone, R. Phillips, D. Kumar, F. Westwell, A. Sturdy, L. Barcella, N. Soussi, M. Mpelembue, S. Raj, R. Sharma, T. Corrah, L. John, A. Whittington, S. Roche, L. Wagstaff, A. Farrier, K. Bisnauthsing, M. Abeywickrama, N. Spence, A. Packham, T. Serafimova, S. Aslam, C. McGreevy, A. Borca, P. DeLosSantosDominguez, E. Palmer, S. Broadhead, S. Farooqi, J. Piper, R. Weighell, L. Pickup, D. Shamtally, J. Domingo, E. Kourampa, C. Hale, J. Gibney, M. Stackpoole, Z. Rashid-Gardner, R. Lyon, C. McDonnell, C. Cole, A. Stewart, G. McMillan, M. Savage, H. Beckett, C. Moorbey, A. Desai, C. Brown, K. Naker, K. Gokani, C. Trinham, C. Sabine, S. Moore, S. Hurdover, E. Justice, M. Stone, E. Plested, C. Ferreira Da Silva, R. White, H. Robinson, I. Turnbull, G. Morshead, R. Drake-Brockman, C. Smith, G. Li, M. Kasanyinga, E. A. Clutterbuck, S. Bibi, M. Singh, T. Champaneri, M. Irwin, M. Khan, A. Kownacka, M. Nabunjo, C. Osuji, J. Hladkiwskyj, D. Galvin, G. Patel, J. Grierson, S. Males, K. Askoolam, J. Barry, J. Mouland, B. Longhurst, M. Moon, B. Giddins, C. Pereira Dias Alves, L. Richmond, C. Minnis, S. Baryschpolec, S. Elliott, L. Fox, V. Graham, N. Baker, K. Godwin, K. Buttigieg, C. Knight, P. Brown, P. Lall, I. Shaik, E. Chiplin, E. Brunt, S. Leung, L. Allen, S. Thomas, S. Fraser, B. Choi, J. Gouriet, J. Perkins, A. Gowland, J. Macdonald, J. P. Seenan, I. Starinskij, A. Seaton, E. Peters, S. Singh, B. Gardside, A. Bonnaud, C. Davies, E. Gordon, S. Keenan, J. Hall, S. Wilkins, S. Tasker, R. James, I. Seath, K. Littlewood, J. Newman, I. Boubriak, D. Suggitt, H. Haydock, S. Bennett, W. Woodyatt, K. Hughes, J. Bell, T. Coughlan, D. van Welsenes, M. Kamal, C. Cooper, S. Tunstall, N. Ronan, R. Cutts, T. Dare, Y. T. N. Yim, S. Whittley, S. Hamal, M. Ricamara, K. Adams, H. Baker, K. Driver, N. Turner, T. Rawlins, S. Roy, M. Merida-Morillas, Y. Sakagami, A. Andrews, L. Goncalvescordeiro, M. Stokes, W. Ambihapathy, J. Spencer, N. Parungao, L. Berry, J. Cullinane, L. Presland, A. Ross Russell, S. Warren, J. Baker, A. Oliver, A. Buadi, K. Lee, L. Haskell, R. Romani, I. Bentley, T. Whitbred, S. Fowler, J. Gavin, A. Magee, T. Watson, K. Nightingale, P. Marius, E. Summerton, E. Locke, T. Honey, A. Lingwood, A. de la Haye, R. S. Elliott, K. Underwood, M. King, S. Davies-Dear, E. Horsfall, O. Chalwin, H. Burton, C. J. Edwards, B. Welham, K. Appleby, E. Dineen, S. Garrahy, F. Hall, E. Ladikou, D. Mullan, D. Hansen, M. Campbell, F. Dos Santos, N. Lakeman, D. Branney, L. Vamplew, A. Hogan, J. Frankham, M. Wiselka, D. Vail, V. Wenn, V. Renals, K. Ellis, J. Lewis-Taylor, H. Habash-Bailey, J. Magan, A. Hardy, Safety, immunogenicity, and reactogenicity of BNT162b2 and mRNA-1273 COVID-19 vaccines given as fourth-dose boosters following two doses of ChAdOx1 nCoV-19 or BNT162b2 and a third dose

of BNT162b2 (COV-BOOST): a multicentre, blinded, phase 2, randomised t. *Lancet Infect. Dis.* **2**, 1131–1141 (2022).

48. N. Andrews, J. Stowe, F. Kirsebom, S. Toffa, T. Rickeard, E. Gallagher, C. Gower, M. Kall, N. Groves, A.-M. O'Connell, D. Simons, P. B. Blomquist, A. Zaidi, S. Nash, N. Iwani Binti Abdul Aziz, S. Thelwall, G. Dabrera, R. Myers, G. Amirthalingam, S. Gharbia, J. C. Barrett, R. Elson, S. N. Ladhani, N. Ferguson, M. Zambon, C. N. J. Campbell, K. Brown, S. Hopkins, M. Chand, M. Ramsay, J. Lopez Bernal, Covid-19 Vaccine Effectiveness against the Omicron (B.1.1.529) Variant. *N. Engl. J. Med.* **386**, 1532–1546 (2022).

49. Y. M. Bar-On, Y. Goldberg, M. Mandel, O. Bodenheimer, O. Amir, L. Freedman, S. Alroy-Preis, N. Ash, A. Huppert, R. Milo, Protection by a Fourth Dose of BNT162b2 against Omicron in Israel. *N. Engl. J. Med.* **386**, 1712–1720 (2022).

50. C. Henry, A. K. E. Palm, F. Krammer, P. C. Wilson, From Original Antigenic Sin to the Universal Influenza Virus Vaccine. *Trends Immunol.* **39**, 70–79 (2018).

51. A. Biswas, A. K. Chakrabarti, S. Dutta, Current challenges: from the path of "original antigenic sin" towards the development of universal flu vaccines: Flu vaccine efficacy encounters significant hurdles from pre-existing immunity of the host suggesting assessment of host immunity before vacci. *Int. Rev. Immunol.* **39**, 21–36 (2020).

52. H. Aoki, M. Tsunoda, H. Ogiwara, H. Shimizu, H. Abe, T. Abe, S. Shichino, K. Matsushima, S. Ueha, Clonal spreading of tumor-infiltrating T cells underlies the robust antitumor immune responses. bioRxiv, 1-59, (2022). doi: https://doi.org/10.1101/2022.04.19.488731.

53. M. Martin, Cutadapt Removes Adapter Sequences From High-Throughput Sequencing Reads. EMBnet.journal. 17, 10–12 (2013). DOI: https://doi.org/10.14806/ej.17.1.200

54. R. Schmieder, R. Edwards, Quality control and preprocessing of metagenomic datasets. *Bioinformatics*. **27**, 863–864 (2011).

55. D. A. Bolotin, S. Poslavsky, I. Mitrophanov, M. Shugay, I. Z. Mamedov, E. V. Putintseva, D. M. Chudakov, MiXCR: Software for comprehensive adaptive immunity profiling. *Nat. Methods*. **12**, 380–381 (2015).

56. H. Aoki, S. Ueha, S. Shichino, H. Ogiwara, K. Shitara, M. Shimomura, T. Suzuki, T. Nakatsura, M. Yamashita, S. Kitano, S. Kuroda, M. Wakabayashi, M. Kurachi, S. Ito, T. Doi, K. Matsushima, Transient depletion of CD4þ cells induces remodeling of the TCR repertoire in gastrointestinal cancer. *Cancer Immunol. Res.* **9**, 624–636 (2021).

57. M. Shugay, D. V. Bagaev, M. A. Turchaninova, D. A. Bolotin, O. V. Britanova, E. V. Putintseva, M. V. Pogorelyy, V. I. Nazarov, I. V. Zvyagin, V. I. Kirgizova, K. I. Kirgizov, E. V. Skorobogatova, D. M. Chudakov, VDJtools: Unifying Post-analysis of T Cell Receptor Repertoires. *PLoS Comput. Biol.* **11**, 1–16 (2015).

58. M. Klinger, F. Pepin, J. Wilkins, T. Asbury, T. Wittkop, J. Zheng, M. Moorhead, M. Faham, Multiplex identification of antigen-specific T cell receptors using a combination of immune assays and immune receptor sequencing. *PLoS One*. **10**, 1–21 (2015).

59. S. Shichino, S. Ueha, S. Hashimoto, T. Ogawa, H. Aoki, B. Wu, C.-Y. Chen, M. Kitabatake, N. Ouji-Sageshima, S. Hontsu, N. Sawabata, T. Kawaguchi, T. Okayama, E. Sugihara, T. Ito, Y. Iwata, T. Wada, K. Ikeo, T. Sato, K. Matsushima, TAS-Seq is a robust and sensitive amplification method for bead-based scRNA-seq. *Commun Biol*, **5(1)**, 602 (2022). doi: 10.1038/s42003-022-03536-0.

60. W. Shen, S. Le, Y. Li, F. Hu, SeqKit: A cross-platform and ultrafast toolkit for FASTA/Q file manipulation. *PLoS One*. **11**, 1–10 (2016).

61. B. Langmead, S. L. Salzberg, Fast gapped-read alignment with Bowtie 2. *Nat. Methods*. **9**, 357–359 (2012).

62. A. T. L. Lun, S. Riesenfeld, T. Andrews, T. P. Dao, T. Gomes, J. C. Marioni, Distinguishing cells from empty droplets in droplet-based single-cell RNA sequencing data. *bioRxiv*, 1–9 (2018).

63. L. Song, L. Florea, B. Langmead, Lighter: fast and memory-efficient sequencing error correction without counting. *Genome Biol.* **15**, 509 (2014).

Acknowledgments: We would like to thank Y. Hara for advice in cell sorting, member of IGT. Inc. for expert technical assistance in TCR sequencing, D. Komura and S. Ishikawa for advice in data analysis. We also thank Dr. David L. Woodland for excellent English language editing. Fig. 1A, B, Fig. 3A, and Fig. 4B were created with BioRender.com.

Funding:

Japan Society for the Promotion of Science, Grant-in-Aid for Scientific Research on Innovative Areas 17929397 (KM)

Japan Society for the Promotion of Science, Grants-in-Aid for Scientific Research 20281832 (SU)

Japan Agency for Medical Research and Development grant, Research Program on Hepatitis JP22fk0310509 (SU)

Japan Agency for Medical Research and Development grant, Project for Cancer Research and Therapeutic Evolution JP22ama221306 (KM)

Japan Agency for Medical Research and Development grant, PRIME program P21gm6210025 (SS)

Author contributions:

Conceptualization: HA, MK, TI, SU

Data curation: HA

Software: HA, SS

Formal analysis: HA

Methodology: HA, SS, AH, SU

Investigation: HA, MK, HA, AH, NOS, SU

Visualization: HA

Funding acquisition: TI, KM, SU

Project administration: TI, SU

Supervision: SS, KM

Writing – original draft: HA, SU

Writing – review & editing: HA, MK, HA, SS, AH, NOS, TI, KM, SU

Competing interests: H.A. reports stock for ImmunoGeneTeqs, Inc. S.S. reports advisory role for ImmunoGeneTeqs, Inc; stock for ImmunoGeneTeqs, Inc, T.I. reports research funding from Rohto Pharmaceutical Co., Ltd. and Biometrics Sympathies Inc. K.M. reports consulting or advisory role for Kyowa-Hakko Kirin, ImmunoGeneTeqs, Inc; research funding from Kyowa-Hakko Kirin, and Ono; stock for ImmunoGeneTeqs, Inc, IDAC Theranostics, Inc. S.U. reports advisory role for ImmunoGeneTeqs, Inc; stock for ImmunoGeneTeqs, Inc, IDAC Theranostics, Inc.

Data and materials availability: All sequencing data (Bulk TCRseq, and Single-cell RNA/TCR sequencing) have been deposited at GEO and are publicly available as of the date of publication (GEO: GSE210231). All original code has been deposited at Github (https://github.com/hiro-aoki-mriid/Covid_TCRrepertoire). The list of antibodies, reagents, and algorithms used in this study was summarized in Tables S5, 6, and 7, respectively.

961 **Figures**:

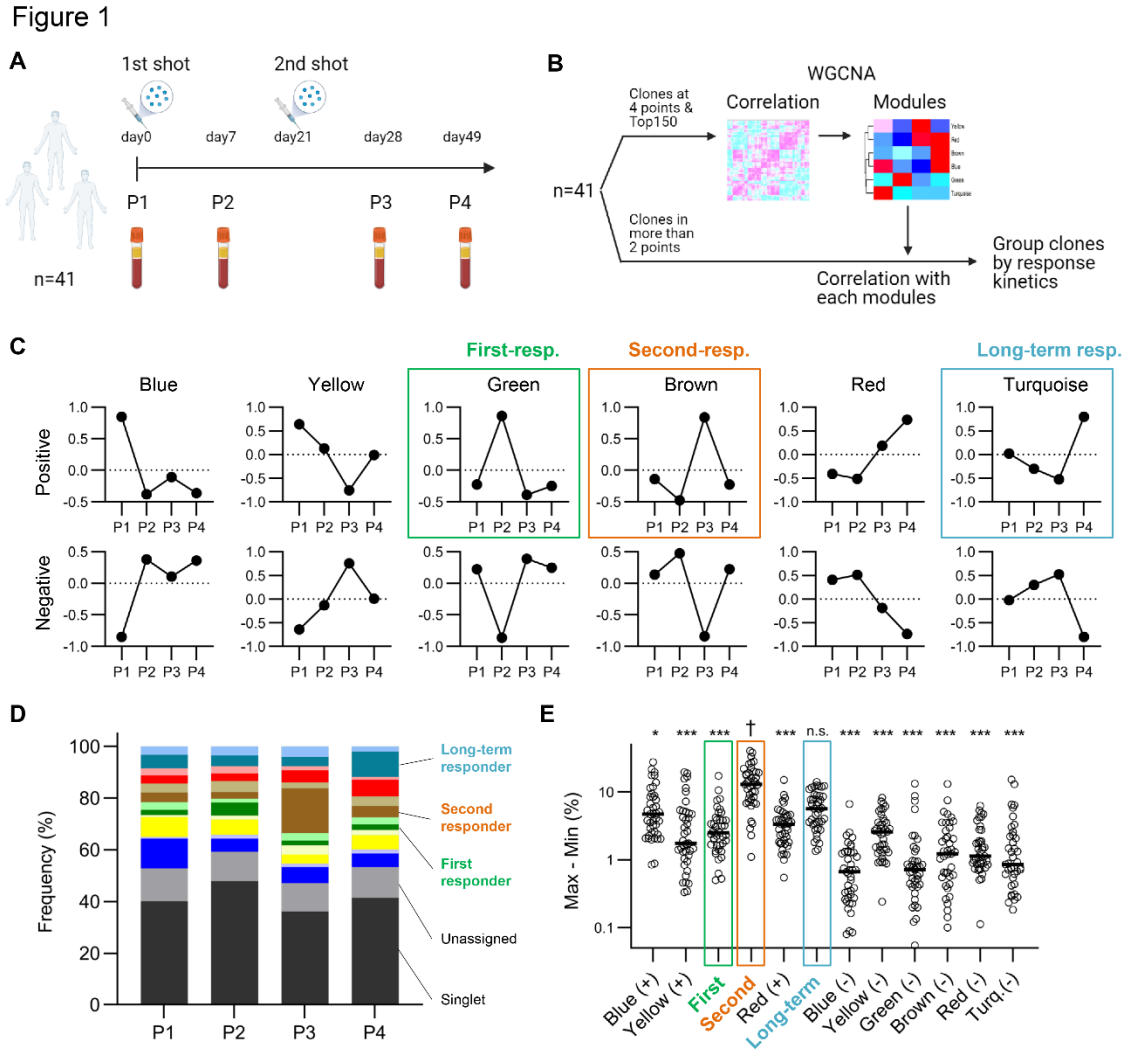

962

963 **Fig. 1**. **Bulk TCR repertoire analysis on blood CD8⁺ T cells.** (**A**) Study design. (**B**) Schematic
964 overview of grouping T-cell clones based on their kinetics profile. The top 150 clones for
965 each participant (150 clones x 41 participants) were selected, and the correlation network
966 of their kinetics profile was generated. Based on this network, modules consisting of
967 highly correlated clones were identified. Then, patterns of kinetics profiles were defined
968 based on the eigenvectors of modules. Finally, clones were classified based on their
969 correlation with each pattern. (**C**) 12 kinetic profile patterns were identified in the $CD8^+$
970 T-cell repertoire. Kinetic profile patterns matching first (module Green (+)), second
971 (module Brown (+)), and long-term responders (module Turquoise (+)) were highlighted.
972 (**D**) Total frequency of $CD8^+$ clones classified into kinetic profile patterns at each time
973 point. Color represents the name of module. (**E**) Comparison of $CD8^+$ clonal response
974 between kinetic profile patterns. The extent of clonal response of each pattern was
975 defined by the maximum changes in their total frequency through P1 to P4. Bars
976 represent the median (n = 41). The mean rank of each pattern was compared with that of

977 pattern Brown (+) (***P<0.001; *P<0.05; n.s. non-significant, Dunn's multiple
978 comparisons test).
979

Figure 2

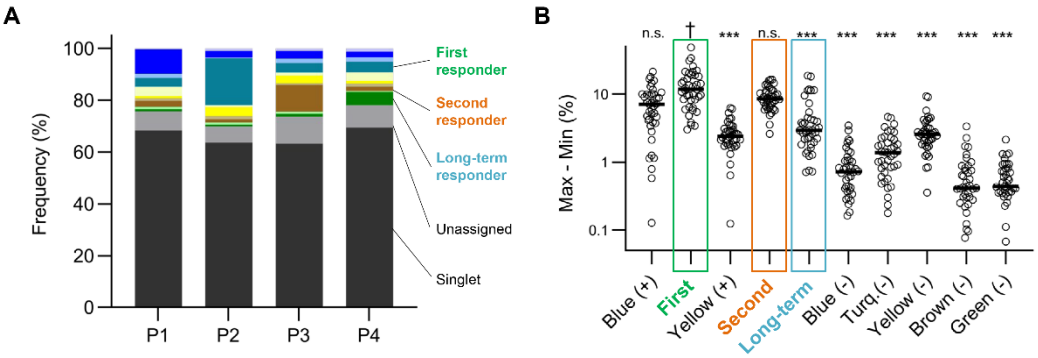

Fig. 2. Bulk TCR repertoire analysis on blood CD4$^+$ T cells. (**A**) Total frequency of CD4$^+$ clones classified to kinetic profile patterns at each time point. Color represents the name of module. (**B**) Comparison of CD4$^+$ clonal response between kinetic profile patterns. The extent of clonal response of each pattern was defined by the maximum changes in their total frequency through P1 to P4. Bars represent the median (n = 41). The mean rank of each pattern was compared with that of pattern Turquoise (+) (***P<0.001; n.s. non-significant, Dunn's multiple comparisons test). First: First responders (module Turquoise (+)). Second: Second responders (module Brown (+)). Long-term: Long-term responders (module Green (+)).

Figure 3

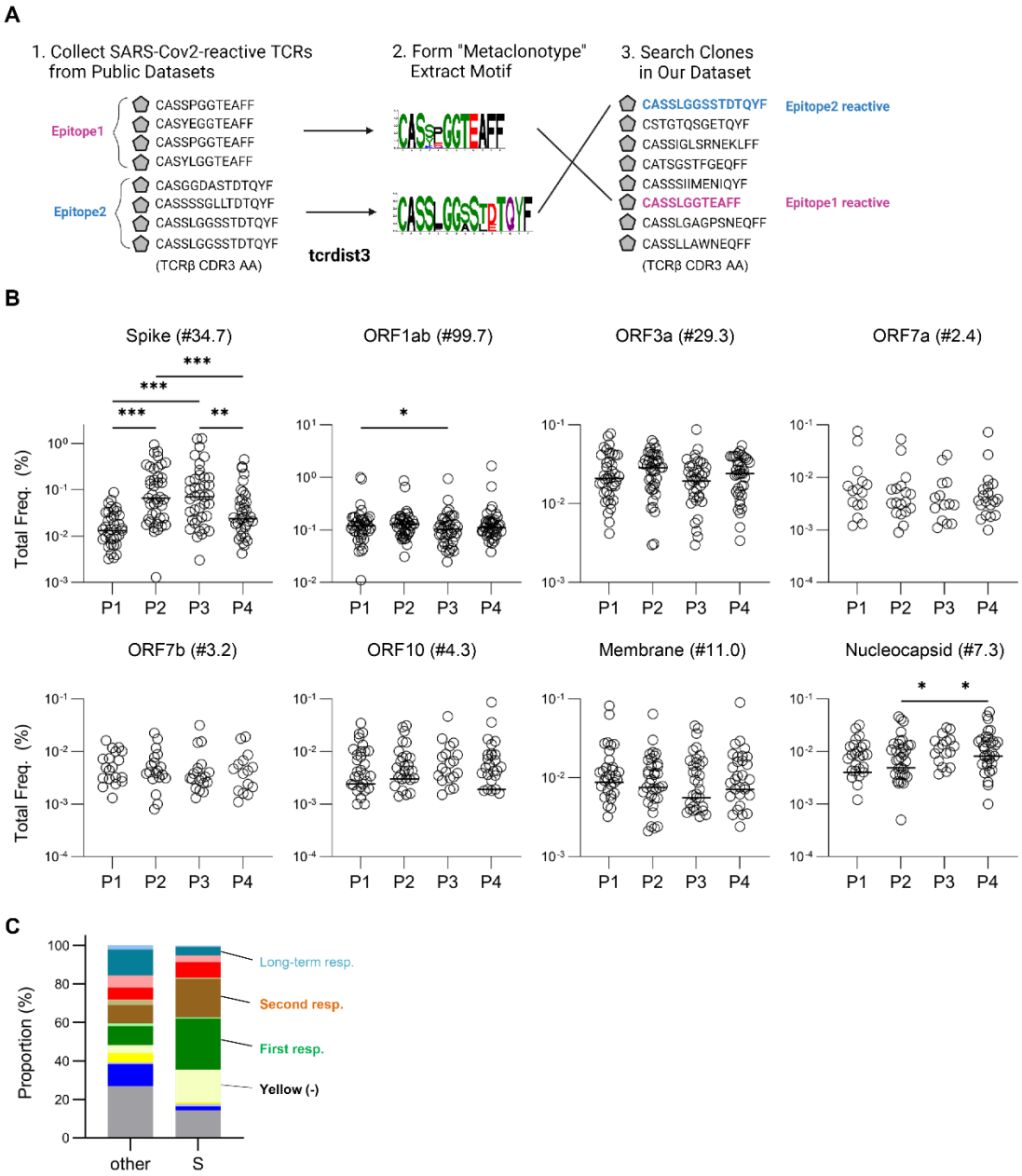

Fig. 3. Searching Spike-reactive TCRs reported in public datasets. (**A**) Schematic overview. (left) We identified TCRs reactive to SARS-CoV-2 epitopes from the three public datasets. (middle) TCR meta-clonotypes were formed for each SARS-CoV-2 epitope. Meta-clonotypes are represented as logo plots, where the sizes and colors of the letters represent the frequency and characteristics of amino acids (red: acidic, blue: basic, green: polar, purple: neutral, black: hydrophobic). (right) TCRs conforming to the definition of meta-clonotypes were searched in our dataset. (**B**) Total frequency of $CD8^+$ SARS-CoV-2 reactive meta-clonotypes at each time point. Bars represent the median (n = 41). Total frequency of meta-clonotypes was compared between time points for each SARS-CoV-2protein (***P<0.001;**P<0.005;*P<0.05, Dunn's multiple comparisons test). (**C**)

1002 Proportion of kinetic profile pattern among clones conformant to Spike-reactive or other
1003 SARS-CoV-2-reactive mata-clonotypes. Color represents the name of module.
1004

Figure 4

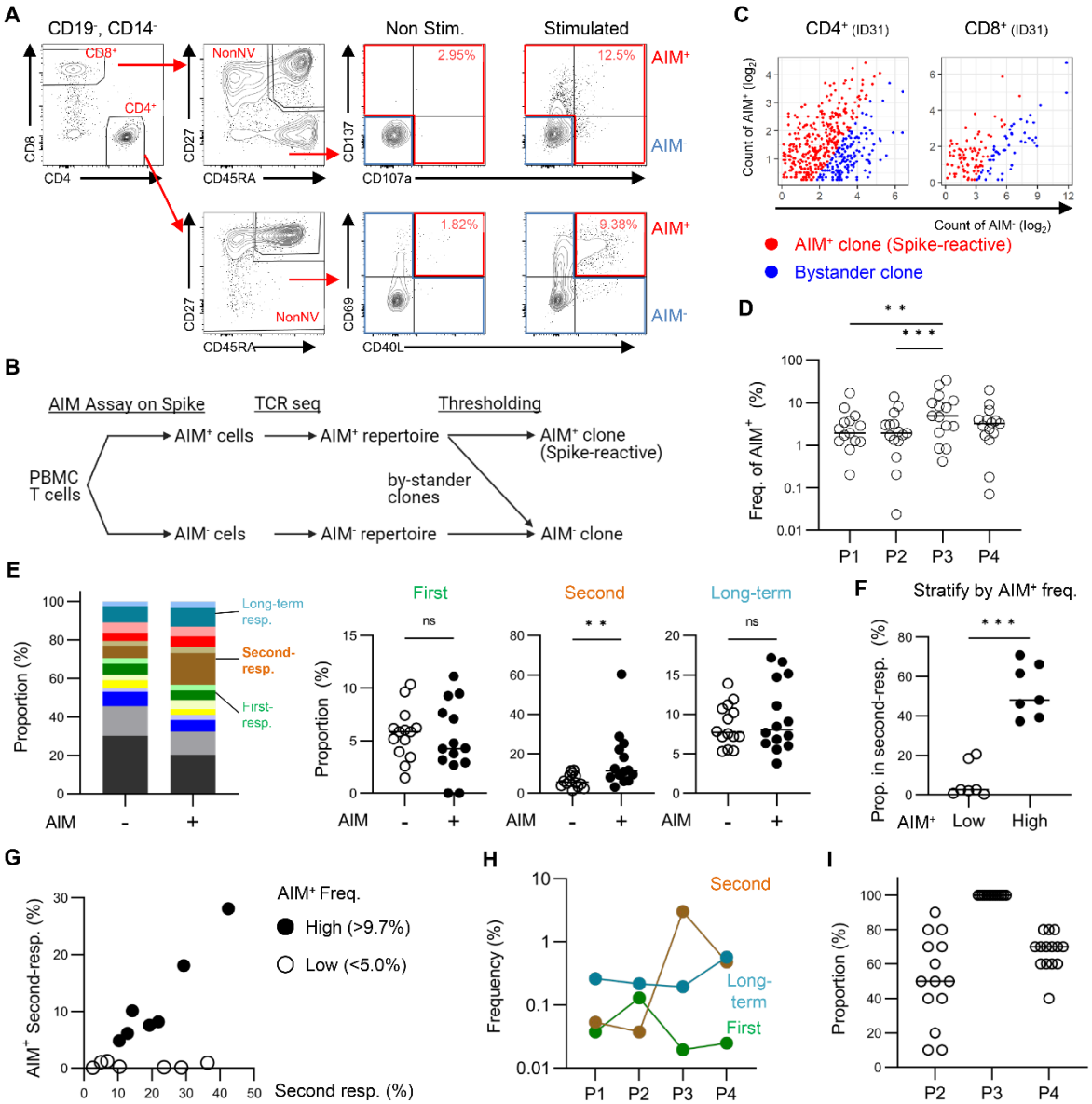

Fig. 4. Analyzing CD8$^+$ Spike-reactive T-cell clones using AIM assay. (**A**) Gating strategy for sorting AIM$^+$ and AIM$^-$ non-naive T cells. Proportion of AIM+ cells among non-naive T cells with or without Spike peptide stimulation was plotted. (**B**) Schematic overview for identifying AIM$^+$ clones. After TCR sequencing on AIM$^+$ and AIM$^-$ T cells, by-stander clones were excluded based on their enrichment in the AIM$^+$ repertoire. (**C**) Scatter plot of overlapping clones between AIM$^+$ and AIM$^-$ repertoire. Individual dots represent clones with their estimated cell count in AIM$^+$ and AIM$^-$ repertoire. (**D**) Comparison of total frequency of CD8$^+$ AIM$^+$ clones between time points (n=15, ***P<0.001;**P<0.005, Dunn's multiple comparisons test). (**E**) (left) Proportion of kinetic profile pattern among CD8$^+$ AIM$^+$ and AIM$^-$ clones. (right) Comparison of the proportion of first-, second-, and long-term responders between CD8$^+$ AIM$^+$ and AIM$^-$ clones (n=14, **P<0.005; n.s. non-significant, Wilcoxon matched-pairs signed rank test).

1018 Color represents the name of module. Participant ID34 was excluded from (E) and the
1019 following analysis, because only two clones were identified as AIM^+ clones. (**F**)
1020 Comparison of the proportion of $CD8^+$ AIM^+ clones among second-responders at P3
1021 between AIM-high and AIM-low participants (n=7 of AIM-high and n=7 of AIM-low,
1022 ***P<0.001, Mann-Whitney test). (**G**) Scatter plot of the frequency of $CD8^+$ second-
1023 responders (x-axis) and AIM^+ second-responders (y-axis). (**H**) Total frequency of $CD8^+$
1024 AIM^+ first-, second-, and long-term responders at each time point. Points represent the
1025 median (n = 14). (**I**) Percentage of $CD8^+$ top 10 AIM^+ clones at P3, which remained top
1026 10 at P2 or P4. (D-F, H, and I) Bars represent the median.
1027

Figure 5

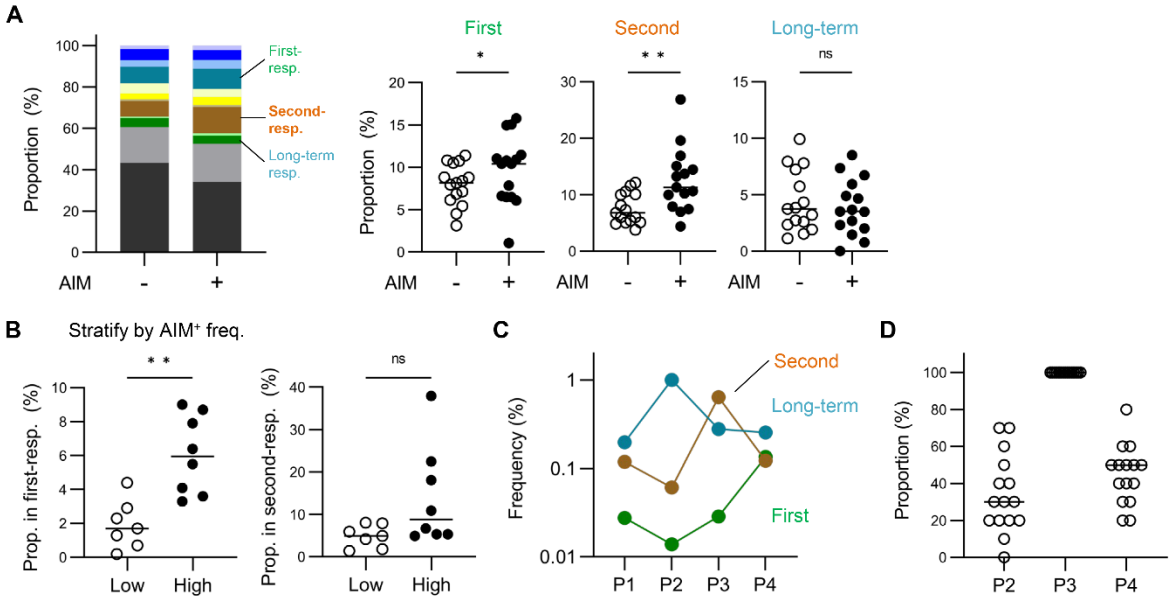

1028

1029 **Fig. 5. Analyzing CD4$^+$ Spike-reactive T-cell clones using AIM assay.** (**A**) (left) Proportion of
1030 kinetic profile pattern among CD4$^+$ AIM$^+$ and AIM$^-$ clones. Color represents the name of
1031 module. (right) Comparison of the proportion of first-, second-, and long-term responders
1032 between CD4$^+$ AIM$^+$ and AIM$^-$ clones (n=15, **P<0.005; *P<0.05; n.s. non-significant,
1033 Wilcoxon matched-pairs signed rank test). (**B**) Comparison of the proportion of CD4$^+$
1034 AIM+ clones among first-responders at P2 (left) or second-responders at P3 (right)
1035 between AIM-high and AIM-low participants (n=7 of AIM-high and n=8 of AIM-low,
1036 **P<0.005; n.s. non-significant, Mann-Whitney test). (**C**) Total frequency of CD4$^+$
1037 AIM+ first-, second-, and long-term responders at each time point. Points represent the
1038 median (n = 15). (**D**) Percentage of CD4$^+$ top 10 AIM+ clones at P3, which remained top
1039 10 at P2 or P4. (A and B) Bars represent the median.
1040

Figure 6

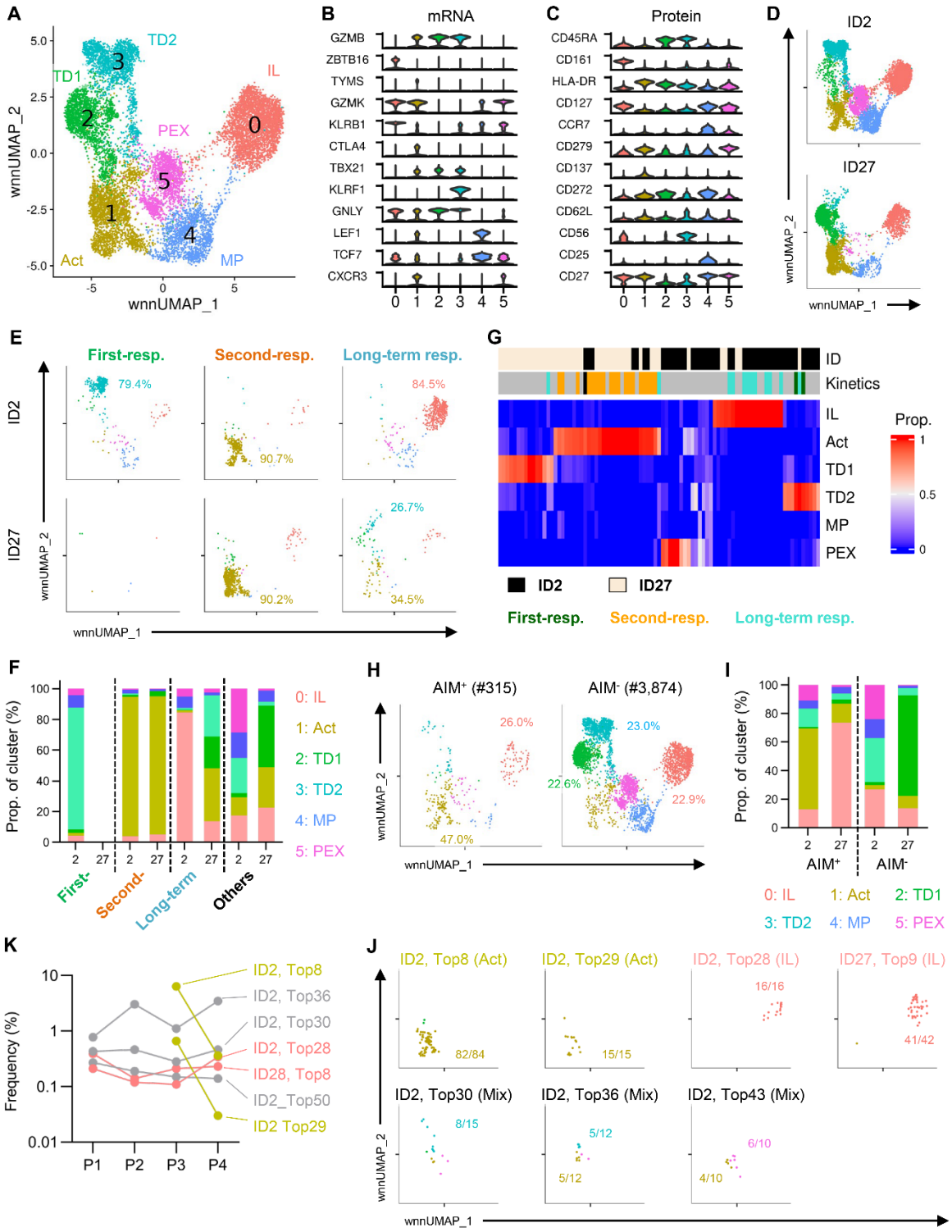

Fig. 6. Single-cell analysis on non-naive CD8$^+$ T cells after the second dose. (**A**) Weighted-nearest neighbor graph-based uniform manifold approximation and projection (wnnUMAP) plot of the scRNAseq/AbSeq data of non-naive CD8$^+$ T cells. (**B** and **C**)

Violin plot showing the mRNA (B) and protein (C) expression of marker genes. (**D**) wnnUmap plot split by the two participants (ID2 and ID27). (**E**) wnnUmap plot for T cells in first-, second-, and long-term responder clones. (**F**) Cluster distribution of T cells in first-, second-, and long-term responder clones. Distribution of T cells in clones with other kinetic profile patterns was also shown ("Other"). (**G**) Heat map for the cluster distribution of expanded clones (≥ 10 cells per clone). Each cell represents the proportion of each cluster (row) in each clone (column). The source ("ID") and kinetic profile ("Kinetics") of clones are also shown as heatmap annotation. (**H**) wnnUmap plot for T cells in AIM^+ or AIM^- clones. Total count of cells in each plot is also shown. (**I**) Cluster distribution of T cells in AIM^+ or AIM^- clones. (**J**) wnnUmap plot for T cells in individual expanded AIM+ clones (≥ 10 cells per clone). Clone name (source, rank in clones detected by scTCR, and dominant phenotype) was shown on the top of the plot. (**K**) Kinetic profile of AIM^+ expanded clones. The frequency of clones at each time point in bulk TCR repertoire data is plotted. IL: innate-like; Act: activated; TD: terminally differentiated; MP: memory precursor; PEX: progenitor exhausted-like.

Figure 7

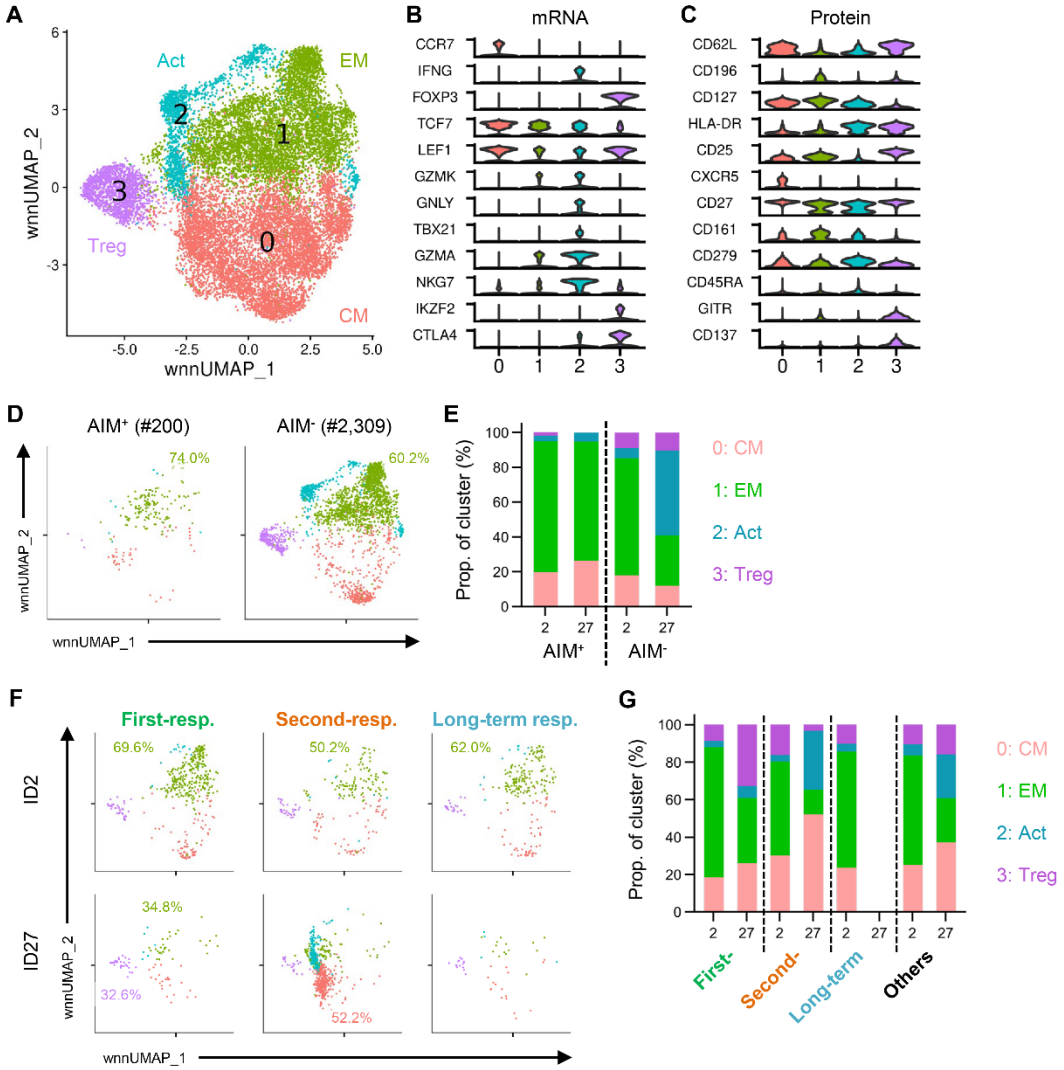

Fig. 7. Single-cell analysis of non-naive CD4$^+$ T cells after the second dose. (**A**) wnnUMAP plot of the scRNAseq/AbSeq data of non-naive CD4$^+$ T cells. (**B** and **C**) Violin plot showing the mRNA (B) and protein (C) expression of marker genes. (**D**) wnnUmap plot for T cells in AIM$^+$ or AIM$^-$ clones. Total count of cells in each plot is also shown. (**E**) Cluster distribution of T cells in AIM$^+$ or AIM$^-$ clones. (**F**) wnnUmap plot for T cells in first-, second-, and long-term responder clones. (**G**) Cluster distribution of T cells in first-, second-, and long-term responder clones. Distribution of T cells in clones with other kinetic profile patterns was also shown ("Other"). CM: central memory; EM: effector memory; Act: activated; Treg: regulatory T cells.